



## **Targeted Delivery of Stk25 Antisense Oligonucleotides to Hepatocytes Protects Mice Against Nonalcoholic Fatty Liver Disease**

Downloaded from: <https://research.chalmers.se>, 2019-09-07 22:09 UTC

Citation for the original published paper (version of record):

Cansby, E., Nuñez-Durán, E., Magnusson, E. et al (2019)

Targeted Delivery of Stk25 Antisense Oligonucleotides to Hepatocytes Protects Mice Against Nonalcoholic Fatty Liver Disease

CMGH Cellular and Molecular Gastroenterology and Hepatology, 7(3): 597-618

<http://dx.doi.org/10.1016/j.jcmgh.2018.12.004>

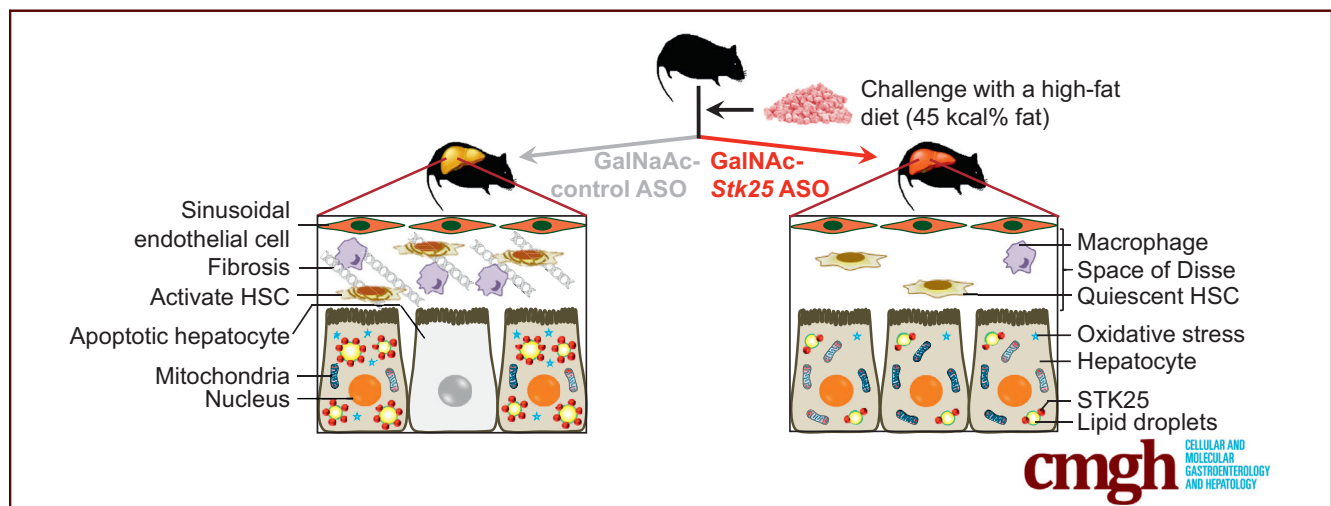
N.B. When citing this work, cite the original published paper.

## ORIGINAL RESEARCH

Targeted Delivery of *Stk25* Antisense Oligonucleotides to Hepatocytes Protects Mice Against Nonalcoholic Fatty Liver Disease

Emmelie Cansby,<sup>1</sup> Esther Nuñez-Durán,<sup>1</sup> Elin Magnusson,<sup>1</sup> Manoj Amrutkar,<sup>2</sup> Sheri L. Booten,<sup>3</sup> Nagaraj M. Kulkarni,<sup>1</sup> L. Thomas Svensson,<sup>4</sup> Jan Borén,<sup>5</sup> Hanns-Ulrich Marschall,<sup>5</sup> Mariam Aghajan,<sup>3</sup> and Margit Mahlapuu<sup>1</sup>

<sup>1</sup>Lundberg Laboratory for Diabetes Research, <sup>5</sup>Wallenberg Laboratory, Department of Molecular and Clinical Medicine, Institute of Medicine, University of Gothenburg, Sahlgrenska University Hospital, Gothenburg, Sweden; <sup>2</sup>Department of Hepato-Pancreato-Biliary Surgery, Institute of Clinical Medicine, University of Oslo, Oslo, Norway; <sup>3</sup>Ionis Pharmaceuticals, Carlsbad, California; <sup>4</sup>Department of Biology and Biological Engineering, National Bioinformatics Infrastructure Sweden, Science for Life Laboratory, Chalmers University of Technology, Gothenburg, Sweden



## SUMMARY

Administration of hepatocyte-specific N-acetylgalactosamine-*Stk25* antisense oligonucleotide (ASO) effectively ameliorated liver steatosis, inflammatory infiltration, and nutritional fibrosis in obese mice. We also observed protection against high-fat-diet-induced hepatic oxidative stress and improved mitochondrial function with *Stk25* ASO treatment. Moreover, N-acetylgalactosamine-*Stk25* ASO suppressed lipogenic gene expression and acetyl-CoA carboxylase protein abundance in the liver, providing insight into the molecular mechanisms underlying repression of hepatic steatosis.

**BACKGROUND & AIMS:** Nonalcoholic fatty liver disease (NAFLD) and nonalcoholic steatohepatitis (NASH) are emerging as leading causes of liver disease worldwide. Currently, no specific pharmacologic therapy is available for NAFLD/NASH, which has been recognized as one of the major unmet medical needs of the 21st century. Our recent studies in genetic mouse models, human cell lines, and well-characterized patient

cohorts have identified serine/threonine protein kinase (STK) 25 as a critical regulator of hepatic lipid partitioning and NAFLD/NASH. Here, we studied the metabolic benefit of liver-specific STK25 inhibitors on NAFLD development and progression in a mouse model of diet-induced obesity.

**METHODS:** We developed a hepatocyte-specific triantennary N-acetylgalactosamine (GalNAc)-conjugated antisense oligonucleotide (ASO) targeting *Stk25* and evaluated its effect on NAFLD features in mice after chronic exposure to dietary lipids.

**RESULTS:** We found that systemic administration of hepatocyte-targeting GalNAc-*Stk25* ASO in obese mice effectively ameliorated steatosis, inflammatory infiltration, hepatic stellate cell activation, nutritional fibrosis, and hepatocellular damage in the liver compared with mice treated with GalNAc-conjugated nontargeting ASO, without any systemic toxicity or local tolerability concerns. We also observed protection against high-fat-diet-induced hepatic oxidative stress and improved mitochondrial function with *Stk25* ASO treatment in mice. Moreover, GalNAc-*Stk25* ASO suppressed lipogenic gene expression and acetyl-CoA carboxylase protein abundance in

the liver, providing insight into the molecular mechanisms underlying repression of hepatic steatosis.

**CONCLUSIONS:** This study provides in vivo nonclinical proof-of-principle for the metabolic benefit of liver-specific inhibition of STK25 in the context of obesity and warrants future investigations to address the therapeutic potential of GalNAc-*Stk25* ASO in the prevention and treatment of NAFLD. (*Cell Mol Gastroenterol Hepatol* 2019;7:597–618; <https://doi.org/10.1016/j.jcmgh.2018.12.004>)

**Keywords:** NAFLD; NASH; Hepatic Steatosis; Liver Fibrosis; Antisense Oligonucleotide Therapy.

See editorial on page 682.

**N**onalcoholic fatty liver disease (NAFLD), defined as the presence of  $\geq 5\%$  of hepatic steatosis in the absence of competing liver disease etiologies or significant alcohol consumption, is emerging as a leading cause of liver disease worldwide. Current estimates indicate that one fifth of adults in the developed world have NAFLD.<sup>1</sup> In a subgroup of patients with NAFLD, the disease progresses to nonalcoholic steatohepatitis (NASH), which in addition to liver steatosis is defined by the presence of hepatic inflammation, fibrosis, and cellular damage in the form of ballooning and apoptosis. NAFLD contributes to the pathogenesis of type 2 diabetes and cardiovascular disease, and patients with NASH are also at high risk of developing cirrhosis, liver failure, and hepatocellular carcinoma.<sup>2,3</sup> To date, there is no established validated therapy for NAFLD/NASH, which is at least partly attributed to an incomplete understanding of the underlying pathogenetic mechanisms and, consequently, a lack of suitable targets.<sup>4</sup>

In the search for novel targets that regulate ectopic lipid accumulation in the context of nutritional stress and obesity, we identified serine/threonine protein kinase (STK)25, a member of the sterile 20 kinase superfamily,<sup>5</sup> as a critical regulator of NAFLD.<sup>6–10</sup> We found that diet-induced NAFLD is exacerbated in mice overexpressing STK25,<sup>7,8</sup> and is prevented in mice with reduced STK25 activity by genetic depletion or antisense oligonucleotide (ASO) treatment.<sup>6,8,10</sup> Furthermore, we have shown that STK25 messenger RNA (mRNA) and protein levels correlate with the severity of NASH in human liver, and several common nonlinked single-nucleotide polymorphisms in the human *STK25* gene are associated with altered liver fat.<sup>8–10</sup> Interestingly, we found that STK25 coats the surface of intrahepatocellular lipid droplets both in human and mouse liver cells.<sup>7,9</sup> Of note, STK25 is broadly expressed<sup>6,11,12</sup> and it also critically regulates lipid partitioning in extrahepatic tissues. Thus, our previous studies have shown that *Stk25* transgenic mice show aggravated diet-induced lipid storage in skeletal muscle, pancreas, and brown and white adipose tissue, which is accompanied by exacerbated inflammatory infiltration and nutritional fibrosis in these tissues, and the reciprocal phenotype is seen in *Stk25*<sup>-/-</sup> mice.<sup>6,13–15</sup>

We also found that overexpression/depletion of STK25 results in increased/reduced atherogenesis susceptibility in a mouse model of hypercholesterolemia.<sup>16</sup>


Because of the broad expression of STK25, our previous experiments using mouse models in which STK25 is globally overexpressed or depleted did not allow us to address whether the impact of STK25 on liver lipid metabolism is direct or secondary to the action of STK25 in extrahepatic tissues. Here, we performed an in vivo nonclinical proof-of-principle study to assess the effect of using the triantennary N-acetylgalactosamine (GalNAc)-conjugated *Stk25* ASO, which results in targeted ASO delivery to hepatocytes, on NAFLD development and progression in obese mice. The results of this study show that reducing STK25 levels selectively in hepatocytes effectively ameliorates progression of liver steatosis, inflammation, fibrosis, and cellular damage in mice in the context of obesity, warranting further investigations of STK25 inhibitors as potential new-in-class drug candidates for the treatment of NAFLD in human beings.

## Results

### GalNAc Conjugation Improves the Liver Potency of *Stk25* ASO

Dosing with generation 2.5 ASOs is known to result in broad systemic target reduction, without penetrating the blood-brain barrier,<sup>17</sup> whereas conjugation of ASOs with a GalNAc moiety leads to efficient and highly selective uptake in hepatocytes.<sup>18</sup> Here, we measured the in vivo efficacy of GalNAc-conjugated *Stk25* ASO (hereafter referred to as GalNAc-*Stk25* ASO) in chow diet-fed mice treated twice weekly for 4 weeks with total doses of 0.15, 0.5, 1.5, or 5.0 mg/kg/wk. At study termination, we observed a dose-dependent reduction of hepatic *Stk25* expression with 90% repression of the target mRNA at the high dose level (5.0 mg/kg/wk) (Figure 1A). As expected, no reduction in *Stk25* mRNA was seen in skeletal muscle of GalNAc-*Stk25* ASO-treated mice at any dose level (Figure 1B). Our previous studies have shown that treatment of chow-fed mice with a corresponding unconjugated generation 2.5 *Stk25* ASO (complementary to the identical 16-nucleotide intronic region of the *Stk25* gene; hereafter referred to as *Stk25* ASO) by similar regimen reduces hepatic *Stk25* expression by

**Abbreviations used in this paper:** 4-HNE, 4-hydroxynonenal; ACC, acetyl-CoA carboxylase; ALT, alanine aminotransferase; ASGP, asialoglycoprotein; ASO, antisense oligonucleotide; ASOR, <sup>125</sup>I-asialo-orosomucoid; AST, aspartate transaminase; DHE, dihydroethidium; GalNAc, N-acetylgalactosamine; mRNA, messenger RNA; NAFLD, nonalcoholic fatty liver disease; NAS, nonalcoholic fatty liver disease activity score; NASH, nonalcoholic steatohepatitis; PBS, phosphate-buffered saline; PCNA, proliferating cell nuclear antigen; STK25, serine/threonine protein kinase 25; TAG, triacylglycerol; TBARS, thiobarbituric acid-reactive substance; WAT, white adipose tissue.

 Most current article

© 2019 The Authors. Published by Elsevier Inc. on behalf of the AGA Institute. This is an open access article under the CC BY-NC-ND license (<http://creativecommons.org/licenses/by-nc-nd/4.0/>).

2352-345X

<https://doi.org/10.1016/j.jcmgh.2018.12.004>

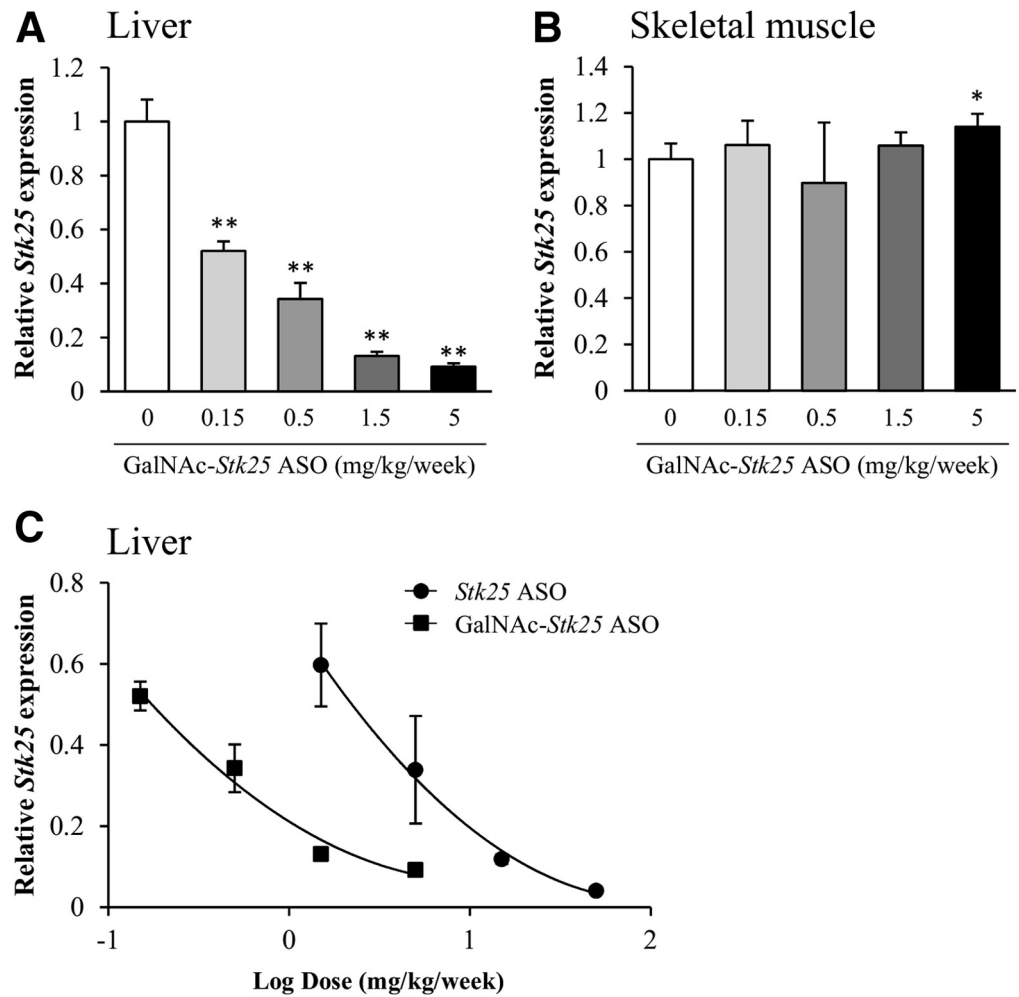


**Figure 1. (A) Dose-dependent reduction of *Stk25* mRNA expression in the liver (B) but not in the skeletal muscle from chow-fed lean mice treated with GalNAc-*Stk25* ASO for 4 weeks. (C) Dose-response curves of *Stk25* ASO and GalNAc-*Stk25* ASO in chow-fed mice. Data are means  $\pm$  SD ( $n = 4$  mice per group) compared with a control group of mice dosed with PBS. \* $P < .05$ , \*\* $P < .01$ .**

90% when using doses of 25–50 mg/kg/wk.<sup>10</sup> The median effective dose (ie, the effective dose required to reduce hepatic *Stk25* levels by 50%) was 0.2 mg/kg/wk for GalNAc-*Stk25* ASO and 2.3 mg/kg/wk for *Stk25* ASO (Figure 1C). Thus, GalNAc conjugation improved the potency of *Stk25* ASO in the liver by approximately 10-fold, similar to that observed with ASOs inhibiting other hepatocyte targets in mice.<sup>18</sup>

Body weight, organ (liver, kidney, and spleen) weights, and plasma chemistry parameters (albumin, bilirubin, blood urea nitrogen, and creatinine) remained within normal reference values in mice treated with GalNAc-*Stk25* ASO (Figure 2A–H). There was high intra-individual variability in plasma alanine aminotransferase (ALT) and aspartate transaminase (AST) measurements; however, all values were in the normal range (ie, well below 100 IU/L for ALT and 200 IU/L for AST), signifying that the GalNAc-*Stk25* ASO was well tolerated (Figure 2I and J). We previously reported similar unremarkable findings in terms of body and organ weights and blood chemistry when using *Stk25* ASO.<sup>10</sup>

### Suppression of Hepatic STK25 by GalNAc-*Stk25* ASO Treatment Effectively Protects Against Liver Steatosis, Macrophage Infiltration, Nutritional Fibrosis, and Hepatocellular Injury in Obese Mice

To show preclinical proof-of-principle for GalNAc-*Stk25* ASO therapy in repressing the progression of NAFLD, we treated diet-induced obese mice with GalNAc-*Stk25* ASO (12.5 mg/kg/wk) and, for comparison, with parent *Stk25* ASO (50 mg/kg/wk), twice weekly for 6 weeks. In addition, GalNAc-conjugated control ASO (12.5 mg/kg/wk), which is a nontargeting ASO of the same length and chemistry as GalNAc-*Stk25* ASO, as well as the phosphate-buffered saline (PBS)-treated group, were included in all experiments (Figure 3). Consistent with previous experience with this class of ASOs,<sup>18</sup> we found that treatment with GalNAc-*Stk25* ASO resulted in significant repression of STK25 levels in the liver, but not in skeletal muscle or white adipose tissue (WAT), of high-fat-fed mice (Figure 4). In contrast, treatment with unconjugated parent *Stk25* ASO resulted in significant reduction of

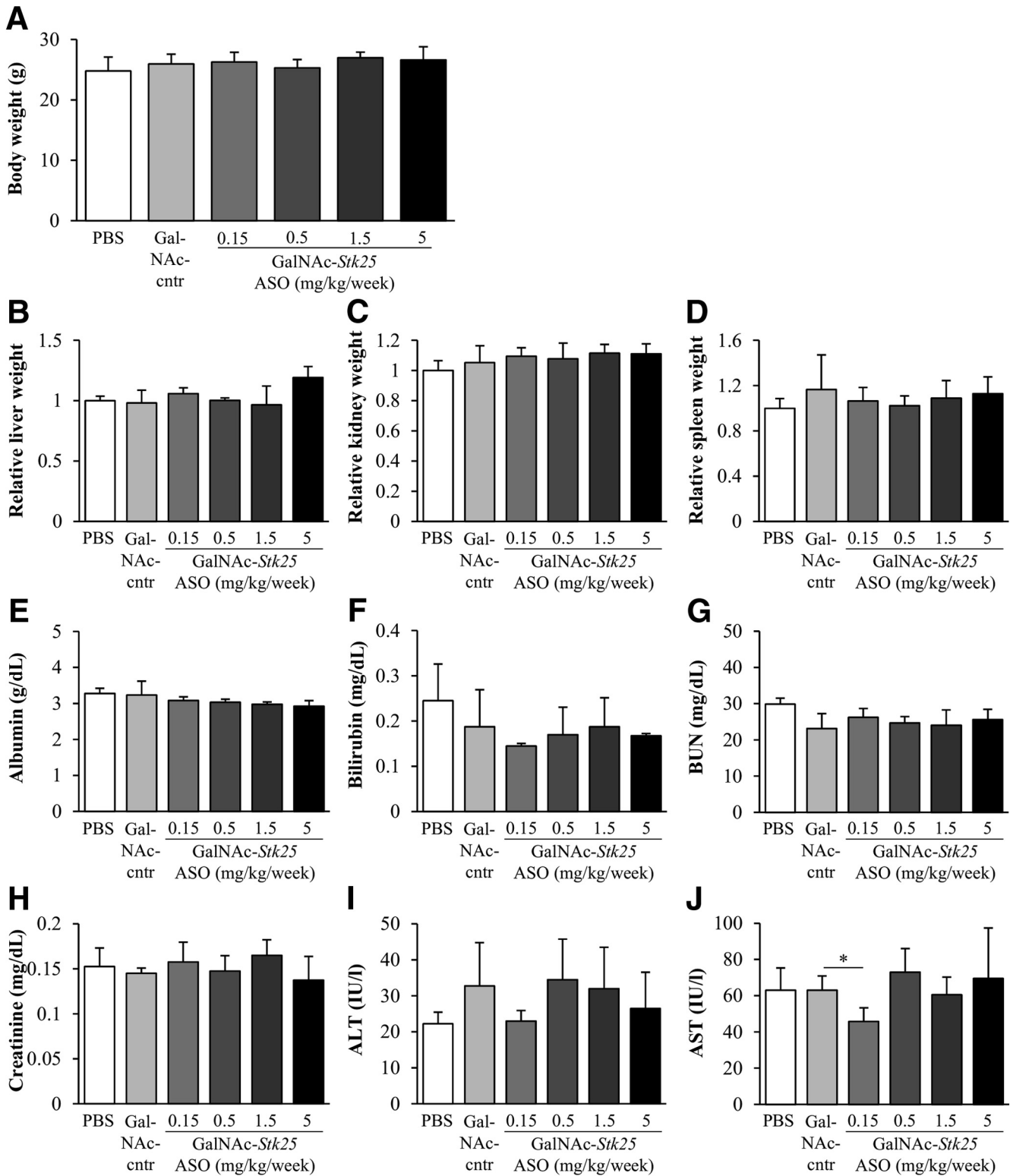


**Figure 2.** Body and organ weights as well as plasma chemistry parameters in chow-fed lean mice dosed with PBS, GalNAc-control ASO, or GalNAc-Stk25 ASO for 4 weeks. (A) Body weight. (B–D) Organ weights; values in control group of mice dosed with PBS are set to 1. (E–J) Plasma chemistry. Data are means ± SD from 4 mice per group. BUN, blood urea nitrogen; cntr, control. \**P* < .05.

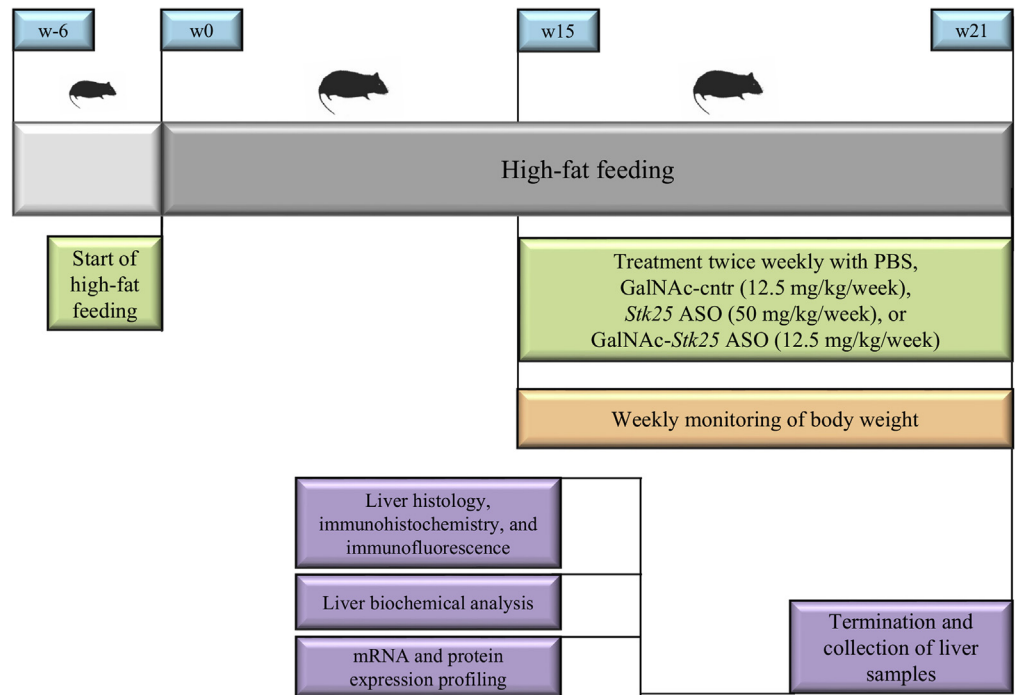


**Figure 3.** Schematic presentation of the experimental design of the in vivo proof-of-principle study to assess the effect of using the GalNAc-conjugated *Stk25* ASO on NAFLD development and progression in obese mice. Cntr, control.

STK25 levels in all tissues examined (ie, in liver, skeletal muscle, and WAT) (Figure 4).

Body weights were similar in all 4 groups of obese mice (Figure 5A); however, food intake was not measured. We observed no difference in general behavior or clinical signs (body posture, mood, and motor activity) comparing the high-fat-fed mice treated with *Stk25*-targeting ASOs vs the control groups, and no local injection-site reactions were recorded. Notably, we found that the homeostasis model assessment score of insulin resistance was improved significantly in obese mice treated with GalNAc-*Stk25* ASO compared with the placebo group of mice (Figure 5B). To study whether repression of STK25 levels induces the risk of hepatocellular carcinoma development, we examined cell proliferation in the liver samples collected from high-fat-diet-fed mice in all 4 treatment groups. We did not detect any increase in hepatic cell proliferation by immunofluorescence or Western blot analysis for commonly used proliferation markers proliferating cell nuclear antigen (PCNA) and Ki67 in mice dosed with *Stk25* ASO or GalNAc-*Stk25* ASO compared with mice treated with PBS or GalNAc-control ASO (Figure 5C and D).

Chronic exposure to dietary lipids is known to promote ectopic lipid storage and meta-inflammation in the liver.<sup>3</sup> Consistently, we found that the livers of high-fat-diet-fed mice treated with PBS or GalNAc-control ASO were visibly lipid-laden with a milky pale appearance (Figure 6A). In contrast, the livers from mice dosed with *Stk25* ASO or GalNAc-*Stk25* ASO were dark red, similar to livers from lean mice fed a regular chow diet (Figure 6A). Microscopic examination of H&E- and Oil Red O-stained liver sections also

showed pronounced steatosis in the 2 control groups of mice, while the density and size of lipid droplets were reduced markedly in mice dosed with *Stk25* ASO or GalNAc-*Stk25* ASO (Figure 6A–C). Similarly, biochemical analysis showed that the hepatic triacylglycerol (TAG) content was significantly lower in the liver extracts from both groups receiving *Stk25*-targeting ASOs (Figure 6D). Notably, the skeletal muscle TAG content was not altered in mice treated with GalNAc-*Stk25* ASO vs GalNAc-control ASO ( $4.8 \pm 1.4$  vs  $5.0 \pm 2.3$   $\mu\text{g}/\text{mg}$  of tissue, respectively).

Hepatic macrophages, which are critical inflammatory mediators in the pathogenesis of NASH, can arise either from circulating monocytes or from self-renewing local macrophages, termed *Kupffer cells*.<sup>19</sup> Both macrophage populations are positive for F4/80, and monocyte-derived macrophages also are characterized by high expression of Gr1 (Ly6C).<sup>19</sup> We found that Gr1 (Ly6C)- and F4/80-positive area was reduced markedly in the livers from mice treated with *Stk25* ASO or GalNAc-*Stk25* ASO compared with mice in both control groups (Figure 7A–C). In fact, we readily observed microgranulomatous lesions and lipogranulomas in the livers from PBS- or GalNAc-control ASO-treated mice (Figure 7D), but not in mice dosed with *Stk25* ASO or GalNAc-*Stk25* ASO, consistent with attenuation of hepatic macrophage infiltration by repression of STK25. Furthermore, repression of STK25 abundance protected from diet-induced perivenular/pericellular fibrosis as shown by staining with Picosirius Red (stains both collagen type I and type III) (Figure 8A) and immunofluorescence analysis for collagen type I (Figure 8A and B). Moreover, immunostaining for  $\alpha$ -smooth muscle actin, a

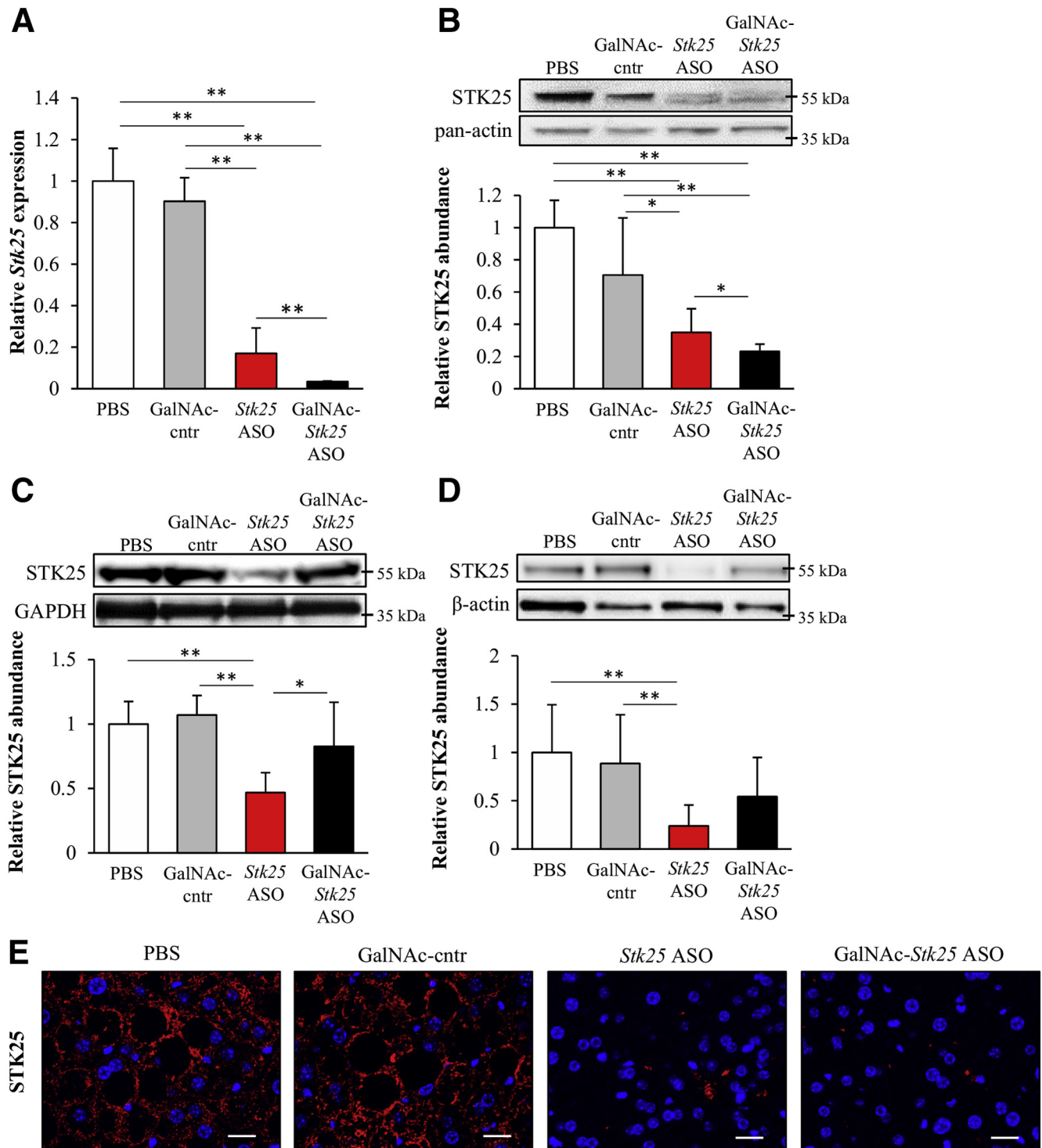
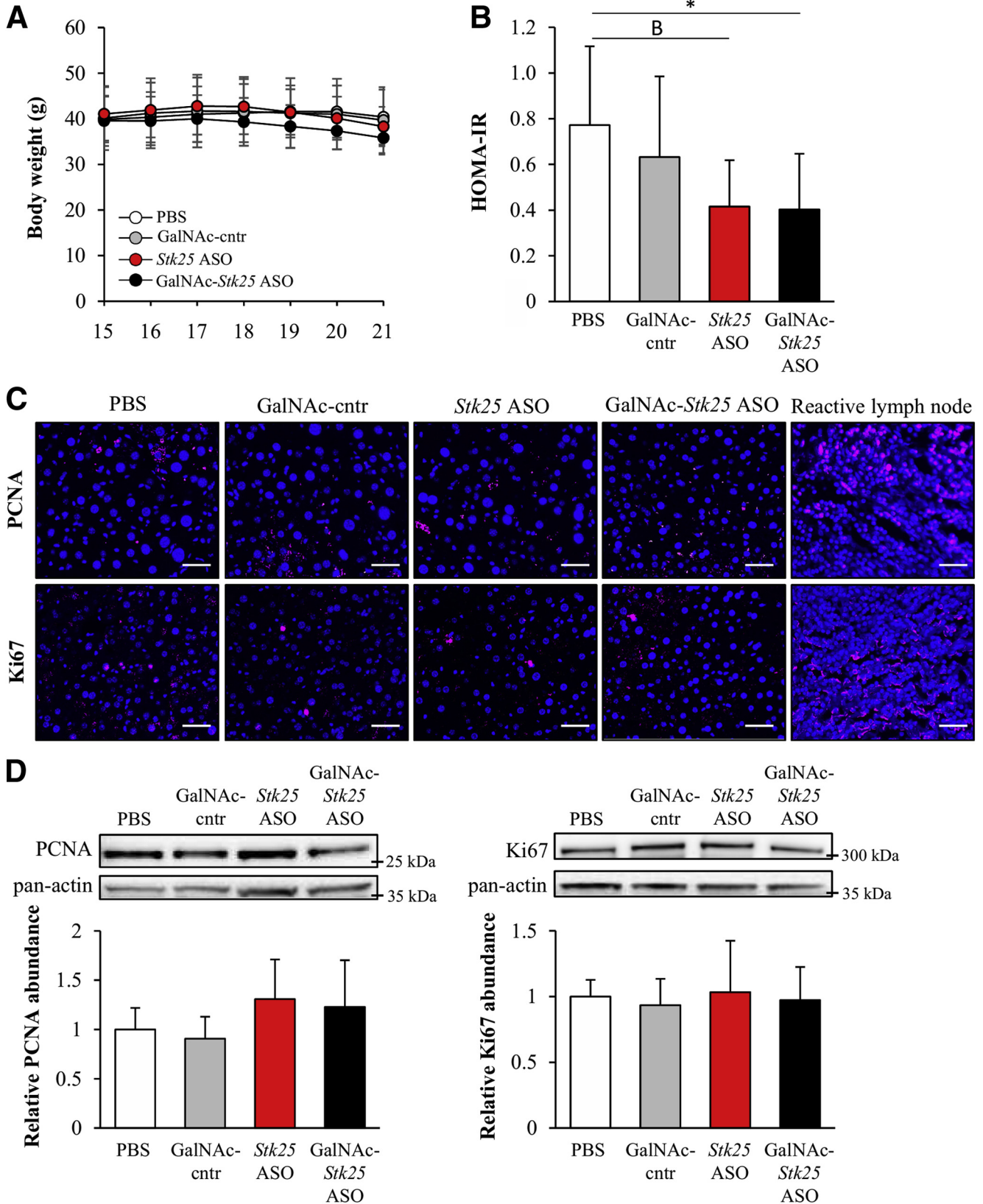


**Figure 4. Treatment of high-fat-diet-fed mice with GalNAc-*Stk25* ASO markedly reduced hepatic STK25 levels.** Mice were treated with GalNAc-*Stk25* ASO (12.5 mg/kg/wk), *Stk25* ASO (50 mg/kg/wk), GalNAc-control ASO (12.5 mg/kg/wk), or placebo (PBS) for 6 weeks. (A) Hepatic *Stk25* mRNA expression. (B–D) STK25 protein abundance in the (B) liver, (C) skeletal muscle, and (D) WAT. Protein levels were analyzed by densitometry; representative Western blots are shown with pan-actin, glyceraldehyde-3-phosphate dehydrogenase (GAPDH), or  $\beta$ -actin used as loading controls. (E) Representative liver sections processed for immunofluorescence with anti-STK25 antibody (red); nuclei were stained with DAPI (blue). Scale bars: 20  $\mu$ m. (A–D) Data are means  $\pm$  SD ( $n = 6$ –8 mice per group) compared with a control group of mice dosed with PBS. Cntr, control. \* $P < .05$ , \*\* $P < .01$ .

marker for activated hepatic stellate cells responsible for liver collagen deposition, similarly was reduced in the livers from mice receiving *Stk25*-targeting ASOs (Figure 8A and C).

Hepatic hydroxyproline content, a marker of collagen deposition, also was lower in liver extracts from mice treated with *Stk25* ASO or GalNAc-*Stk25* ASO (Figure 8D).





Consistent with suppression of hepatic macrophage infiltration and collagen accumulation by GalNac-*Stk25* ASO treatment, we found reduced mRNA expression of several markers of inflammation and fibrinogenesis in livers from mice dosed with GalNac-*Stk25* ASO (Figure 9A and B).

Evidence of hepatocellular damage was readily observed in the livers from control groups of mice, as shown by the presence of apoptotic hepatocytes (detected by terminal deoxynucleotidyl transferase-mediated deoxyuridine triphosphate nick-end labeling assay [TUNEL]) and Mallory bodies (shown by immunostaining for ubiquitin) (Figure 10), as well as enlarged nuclei containing intranuclear vacuoles and ballooning degradation of hepatocytes (Figure 7D); we did not detect these features in mice receiving *Stk25* ASO or GalNac-*Stk25* ASO.

### Treatment With GalNac-*Stk25* ASO Reverses Diet-Induced NAFLD in Mice

We assessed the liver histopathology in high-fat-diet-fed mice by using the NAFLD activity score (NAS) and fibrosis scoring based on the Kleiner/Brunt criteria adapted to rodents.<sup>20–24</sup> Mice dosed with *Stk25* ASO or GalNac-*Stk25* ASO scored significantly lower both for NAS and fibrosis compared with mice receiving PBS or GalNac-control ASO, with the most pronounced improvement seen in the GalNac-*Stk25* ASO-treated group (Figure 11A–C). Interestingly, plasma ALT and AST levels, the most widely used clinical biomarkers of NAFLD/NASH, were reduced significantly in obese mice treated with GalNac-*Stk25* ASO compared with baseline values measured before initiation of ASO treatment, suggesting that STK25 inhibition not only prevents but also reverses diet-induced NAFLD (Figure 11D and E).

### *Stk25* Targeting ASOs Reduce Oxidative Stress and Improve Mitochondrial Function in Mouse Liver

Oxidative stress plays a crucial role in NASH progression.<sup>25</sup> We found that the levels of 4-hydroxynonenal (4-HNE), an end-product of peroxidation of membrane *N*-6-polyunsaturated fatty acids and considered a reliable biomarker of oxidative liver damage, and the dye dihydroethidium (DHE), which detects superoxide radicals ( $O_2^{\cdot -}$ ), were significantly lower in the livers from obese mice treated with *Stk25*-targeting ASOs compared with mice in the control groups (Figure 12A–C). Moreover, we observed suppressed thiobarbituric acid-reactive

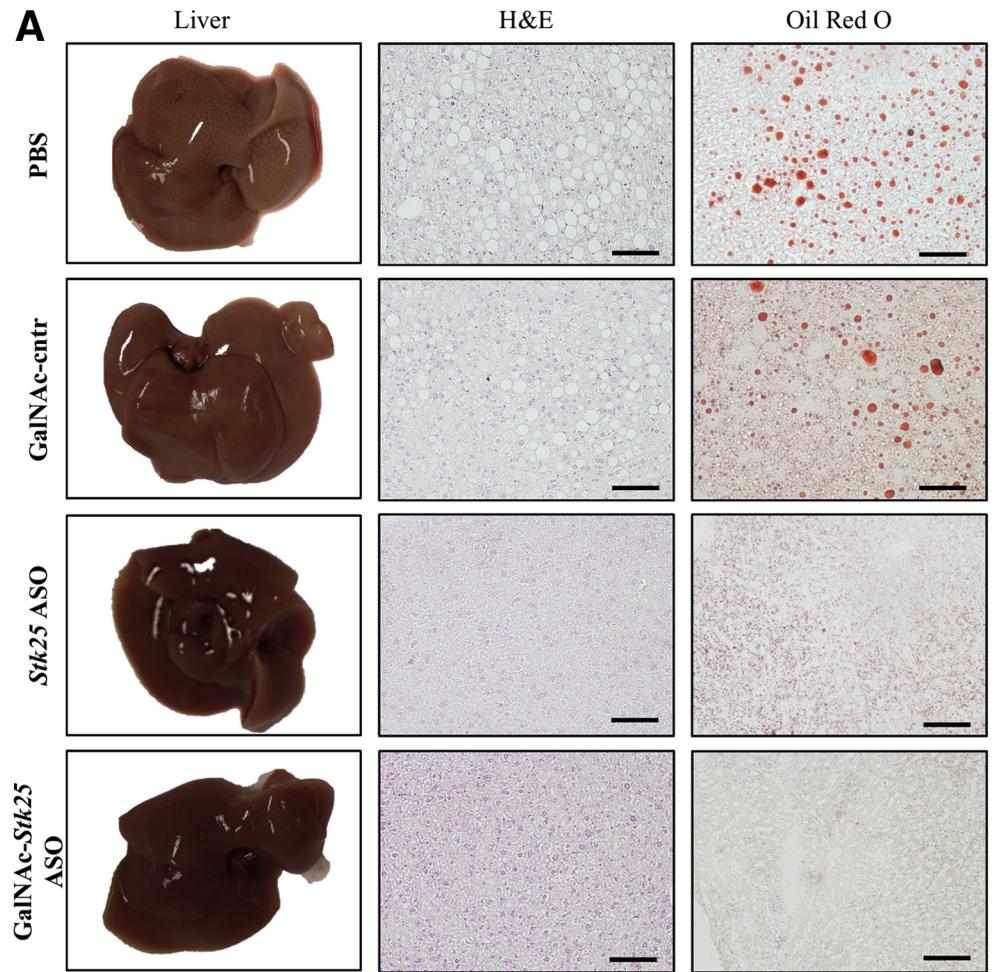
substance (TBARS) content, a classic marker of lipid peroxidation, in the liver extracts from mice dosed with *Stk25* ASO or GalNac-*Stk25* ASO (Figure 12D).

Several lines of evidence suggest that mitochondrial dysfunction, and activation of an alternative extra-mitochondrial fatty acid oxidation pathway in peroxisomes, are the leading mechanisms that promote hepatic oxidative stress.<sup>3,25–27</sup> Interestingly, we found that staining with MitoTracker Red, a fluorescent dye that specifically accumulates within respiring mitochondria, was approximately 3-fold higher in the liver sections from mice treated with *Stk25*-targeting ASOs compared with mice in the control groups (Figure 12A and E). Consistently, we found that the rate of  $\beta$ -oxidation was increased significantly in primary hepatocytes isolated from naive mice of the same strain, when treated in vitro with GalNac-*Stk25* ASO vs GalNac-control ASO ( $42.0 \pm 9.2$  vs  $26.4 \pm 5.0$  pmol/min/mg, respectively;  $P < .01$ ). Reciprocally, immunostaining for peroxisome biogenesis marker PEX5 was approximately 2.5-fold lower in the livers from mice dosed with *Stk25* ASO or GalNac-*Stk25* ASO compared with PBS or GalNac-control ASO (Figure 12A and F).

### Suppression of Lipogenic Gene Expression and Acetyl-CoA Carboxylase Protein Abundance in Livers From Mice Treated With GalNac-*Stk25* ASO

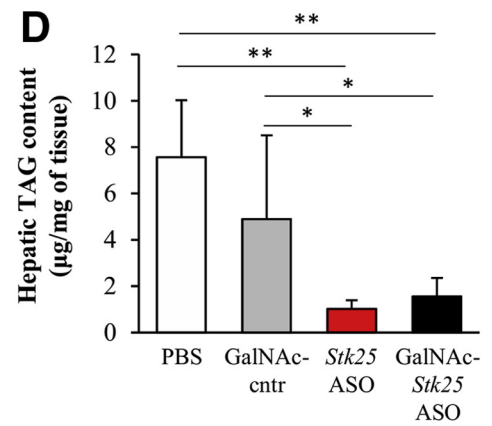
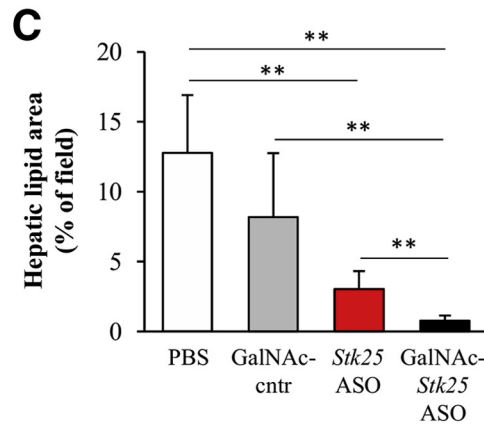
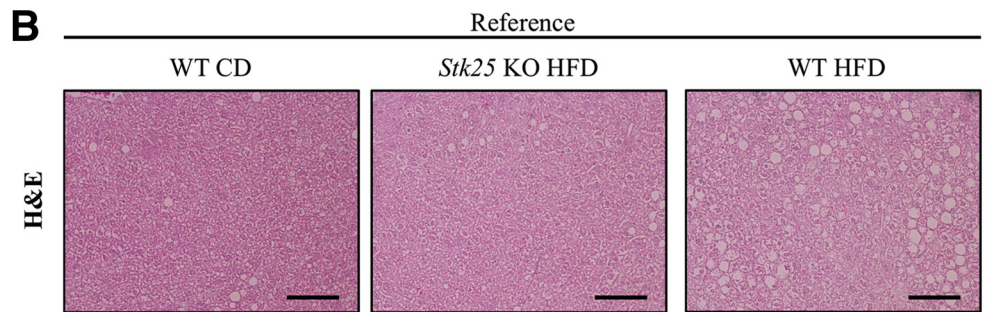
Because the treatment with *Stk25*-targeting ASOs effectively protected against hepatic steatosis, we examined the expression of a set of genes involved in lipogenesis in the livers from all 4 groups of high-fat-fed mice. We found that the hepatic mRNA levels of *Acc1* and *Acly* controlling de novo fatty acid synthesis, as well as *Gpam* and *Hmgcr* regulating TAG and cholesterol biosynthesis, respectively, were down-regulated by approximately 2- to 3-fold in the livers from mice treated with GalNac-*Stk25* ASO (Figure 9C). Interestingly, although the expression of *Gpam* was lower in mice treated with both *Stk25*-targeting ASOs compared with both control groups, the mRNA levels of *Acc1*, *Acly*, and *Hmgcr* were reduced only in the livers from GalNac-*Stk25* ASO-treated mice (Figure 9C), providing a likely mechanism for the improved efficacy of GalNac-conjugated *Stk25* ASO in suppressing hepatic lipid accumulation compared with unconjugated parent *Stk25* ASO. Next, we examined the expression of enzymes regulating hepatic lipid oxidation. From the rate-limiting enzymes studied, only the mRNA expression of *Acc2*, which represses lipid oxidation through

**Figure 5.** (See previous page). Treatment with GalNac-*Stk25* ASO had no impact on body weight gain or liver cell proliferation in mice fed a high-fat diet, whereas the whole-body insulin sensitivity was improved. Mice were treated with GalNac-*Stk25* ASO (12.5 mg/kg/wk), *Stk25* ASO (50 mg/kg/wk), GalNac-control ASO (12.5 mg/kg/wk), or placebo (PBS) for 6 weeks. (A) Body weight curves; the number of weeks on a high-fat diet is shown (the treatment was initiated at week 15 of high-fat diet feeding). (B) The homeostasis model assessment score of insulin resistance (HOMA-IR) was calculated using the following equation: fasting glucose (mg/dL)  $\times$  fasting insulin (ng/mL)/405. (C) Representative liver sections processed for immunofluorescence with anti-PCNA (pink) or anti-Ki67 antibodies (pink); nuclei were stained with DAPI (blue). A histologic section of reactive lymph node (T2235161-3; Gentaur, Brussels, Belgium) was used as positive control for PCNA and Ki67 staining. Scale bars: 40  $\mu$ m. (D) Liver protein lysates were analyzed by Western blot using antibodies specific for PCNA or Ki67. Protein levels were analyzed by densitometry; representative Western blots are shown with pan-actin used as a loading control. (A, B, and D) Data are means  $\pm$  SD from 6–8 mice per group. Cntr, control. \* $P < .05$ , <sup>B</sup> $P = .052$ .



**Figure 6. GalNAc-*Stk25* ASO treatment ameliorated liver steatosis in obese mice.**

Mice were treated with GalNAc-*Stk25* ASO (12.5 mg/kg/wk), *Stk25* ASO (50 mg/kg/wk), GalNAc-control ASO (12.5 mg/kg/wk), or placebo (PBS) for 6 weeks. (A) Representative images of whole liver; representative liver sections stained with H&E or Oil Red O for lipids. (B) Representative liver sections stained with H&E from age-matched chow diet-fed lean mice as well as *Stk25* knockout mice and their wild-type littermates fed a high-fat diet. *Stk25* knockout mice were a gift from B. Howell (State University of New York Upstate Medical University, Syracuse, NY). (C) Quantification of total lipid area in liver sections. (D) TAG content in liver extract. (C and D) Data are means  $\pm$  SD from 6–8 mice per group. Scale bars: 100  $\mu$ m. CD, chow diet; cntr, control; HFD, high-fat diet; KO, knockout; WT, wild-type. \* $P < .05$ , \*\* $P < .01$ .



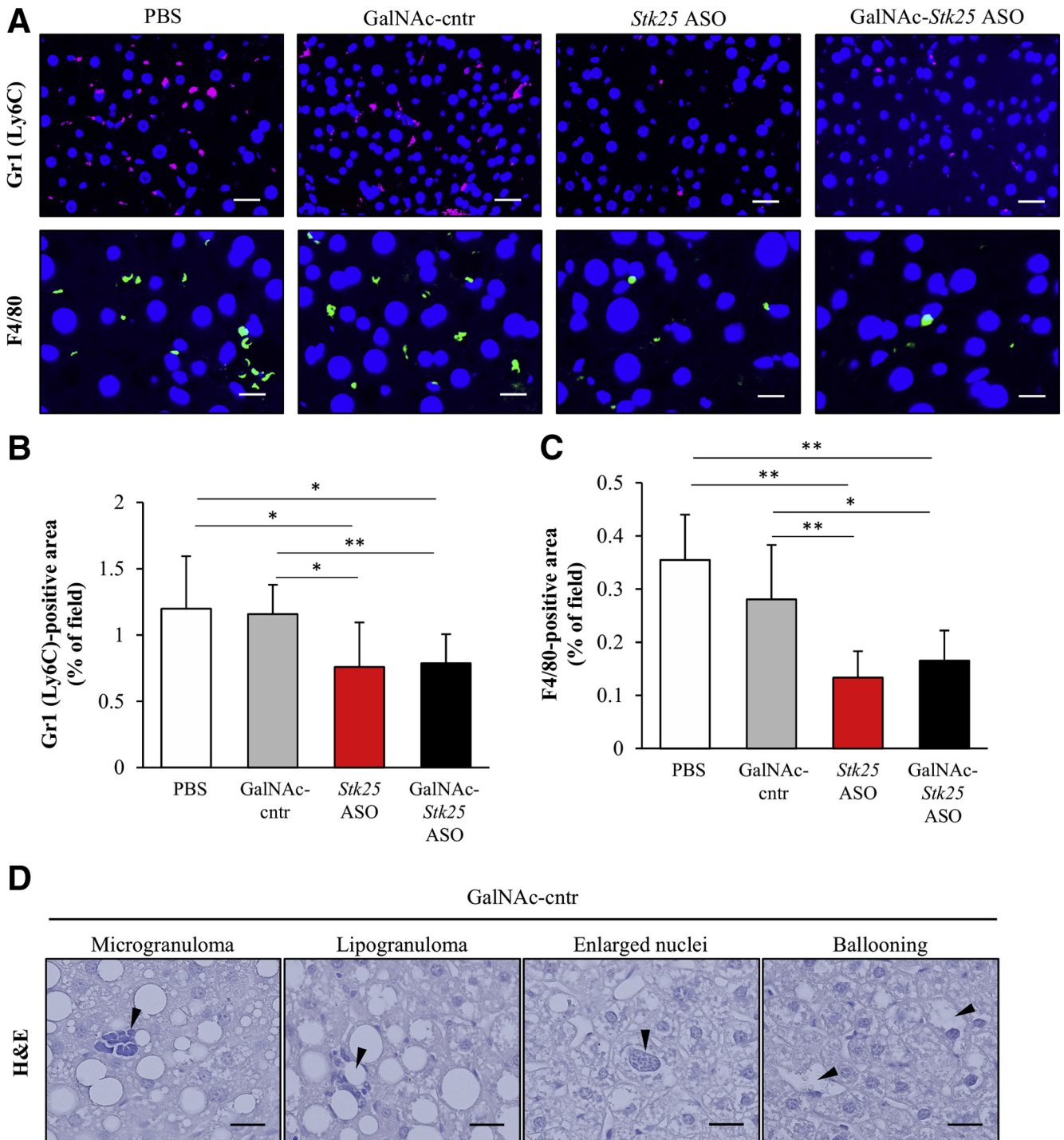


**Figure 7. Treatment with GalNAc-*Stk25* ASO protected against high-fat-diet-induced liver inflammation in mice.** Mice were treated with GalNAc-*Stk25* ASO (12.5 mg/kg/wk), *Stk25* ASO (50 mg/kg/wk), GalNAc-control ASO (12.5 mg/kg/wk), or placebo (PBS) for 6 weeks. (A) Representative liver sections processed for immunofluorescence with anti-Gr1 (Ly6C) (pink) or anti-F4/80 antibodies (green); nuclei were stained with DAPI (blue). Scale bars: 25  $\mu$ m for Gr1 (Ly6C) and 12.5  $\mu$ m for F4/80. (B and C) Quantification of (B) Gr1 (Ly6C) and (C) F4/80 staining. (D) H&E-stained liver sections of mice dosed with GalNAc-control ASO showing the presence of microgranuloma and lipogranuloma, enlarged nuclei containing intranuclear vacuoles, and hepatocellular ballooning. Scale bars: 100  $\mu$ m. (B and C) Data are means  $\pm$  SD from 7–8 mice per group. Cntr, control. \* $P < .05$ , \*\* $P < .01$ .

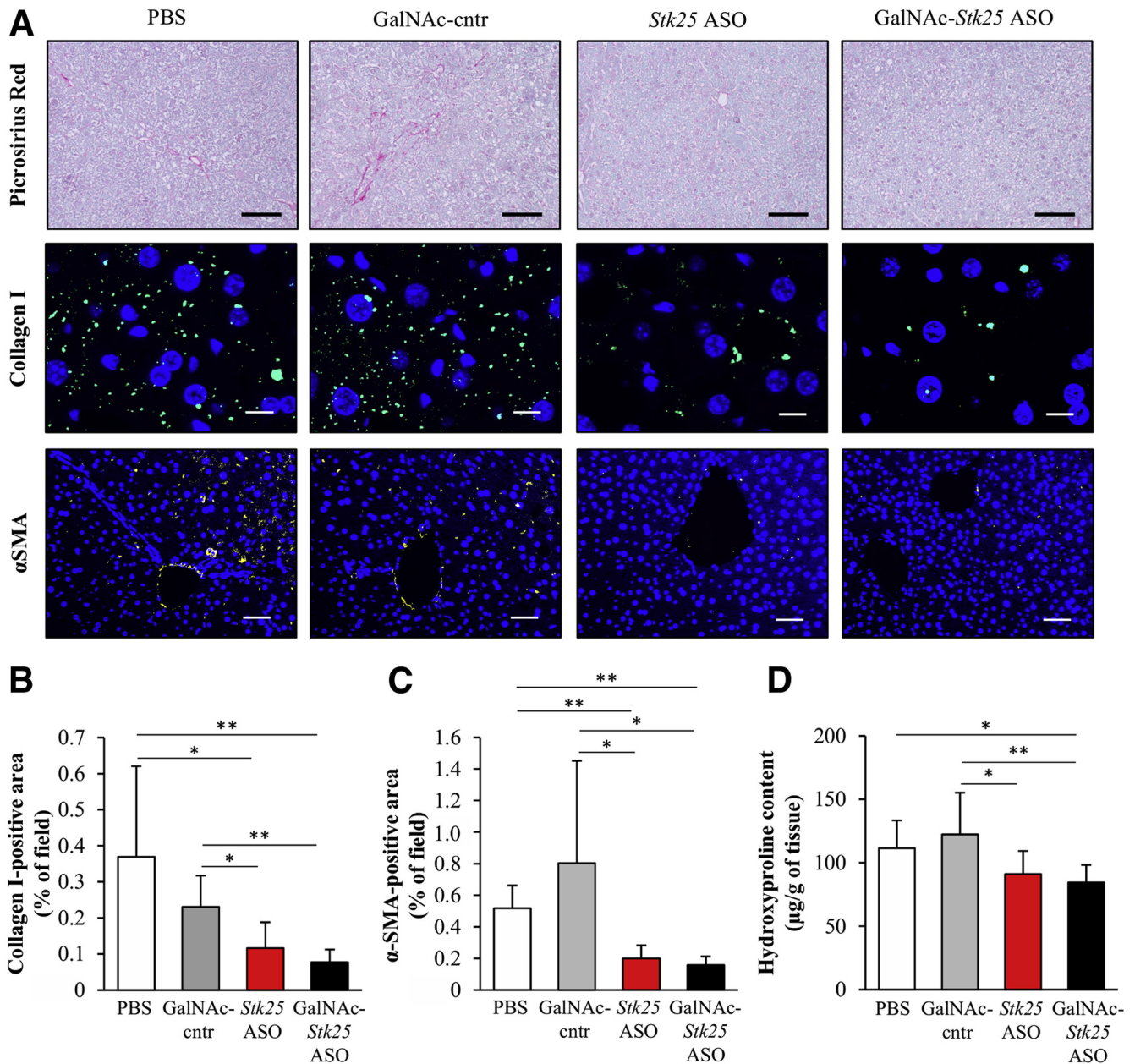


**Figure 8. Administration of GalNac-Stk25 ASO effectively reduced nutritional fibrosis in obese mice.** Mice were treated with GalNac-Stk25 ASO (12.5 mg/kg/wk), Stk25 ASO (50 mg/kg/wk), GalNac-control ASO (12.5 mg/kg/wk), or placebo (PBS) for 6 weeks. (A) Representative liver sections stained with Picrosirius Red or processed for immunofluorescence with anti-collagen I (green) or anti- $\alpha$ -smooth muscle actin ( $\alpha$ -SMA) antibodies (yellow); nuclei were stained with DAPI (blue). Scale bars: 100  $\mu$ m for Picrosirius Red, 12.5  $\mu$ m for collagen I, and 50  $\mu$ m for  $\alpha$ -SMA. (B and C) Quantification of (B) collagen I and (C)  $\alpha$ -SMA staining. (D) Hydroxyproline content in liver extract. (B–D) Data are means  $\pm$  SD from 6–8 mice per group. Cntr, control. \* $P < .05$ , \*\* $P < .01$ .

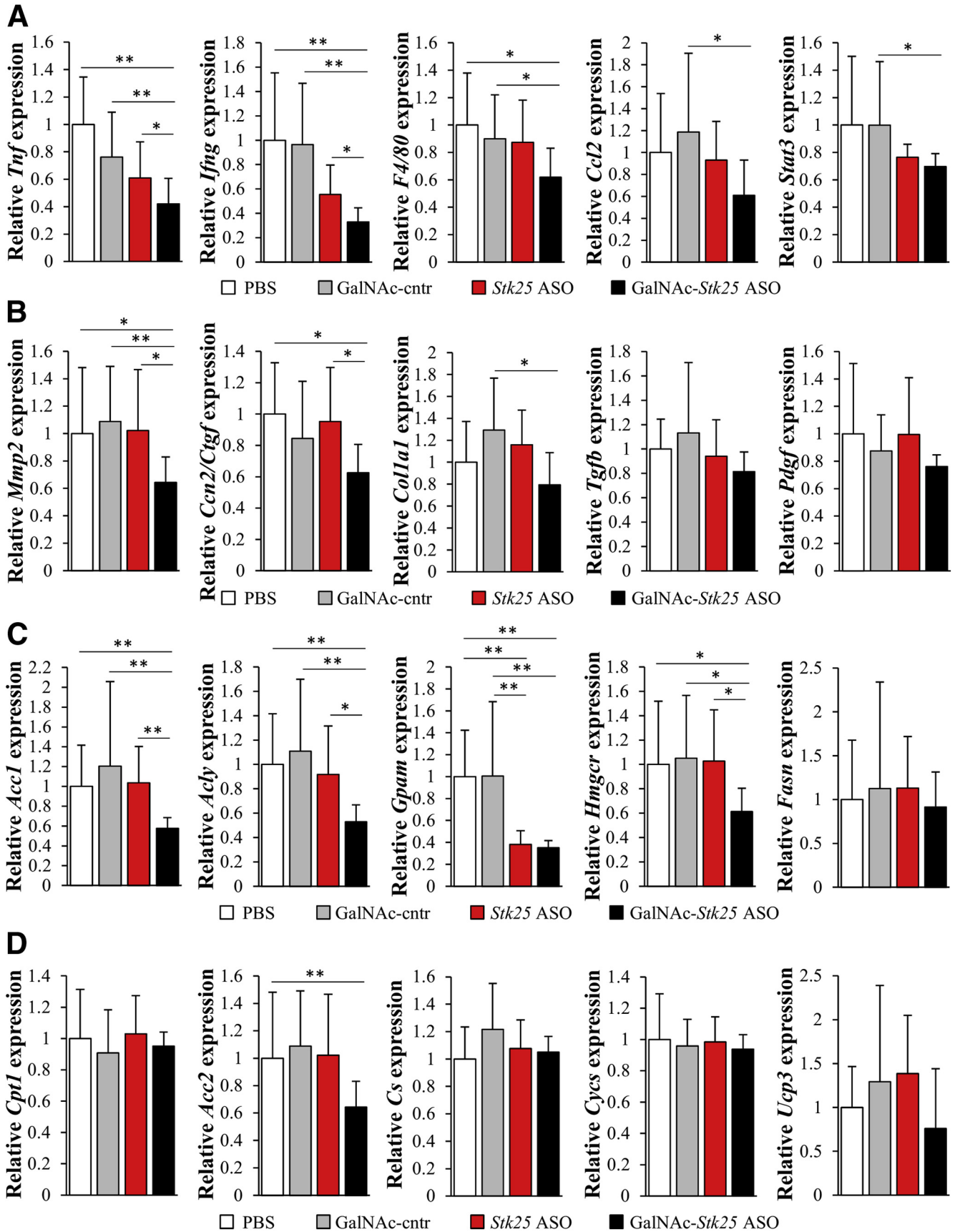
allosteric inhibition of mitochondrial fatty acid transporter carnitine palmitoyltransferase 1 (CPT1),<sup>28</sup> was altered significantly in the livers from mice dosed with GalNac-Stk25 ASO (approximately 1.5-fold lower compared with controls) (Figure 9D).

Consistent with our finding of reduced mRNA expression of *Acc1/2*, the total protein level of acetyl-CoA carboxylase (ACC) was 2.0-  $\pm$  1.0-fold lower in the livers from high-fat-fed mice treated with GalNac-Stk25 ASO compared with

GalNac-control ASO (Figure 13A). The ratio of phospho-ACC (inactive form)/ACC was not altered significantly in comparing these 2 groups (Figure 13A).

#### *STK25 Is Activated in the Liver by Starvation and Challenge With a High-Fat Diet*

The phosphorylation level of the threonine 174 residue of STK25 has been shown to adequately reflect the activity



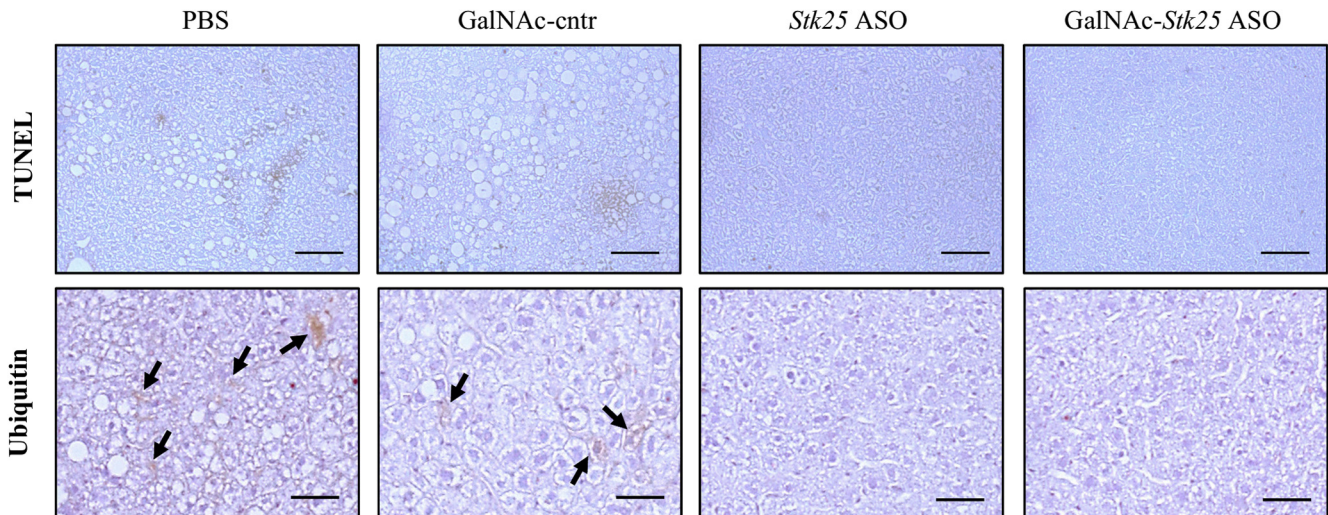


**Figure 10.** Apoptotic hepatocytes (detected by terminal deoxynucleotidyl transferase-mediated deoxyuridine triphosphate nick-end labeling [TUNEL] assay) and Mallory bodies (shown by immunostaining for ubiquitin *black arrows*) were readily observed in the livers from control groups of high-fat-fed mice, but not in mice receiving *Stk25* ASO (50 mg/kg/wk) or GalNAc-*Stk25* ASO (12.5 mg/kg/wk). Representative liver sections stained with TUNEL or processed for immunohistochemistry with anti-ubiquitin antibody (brown). Scale bars: 100  $\mu$ m. Cntr, control.

of this kinase.<sup>29</sup> Notably, we and other research groups previously have shown that inflammatory and oxidative stress increase the threonine 174 phosphorylation of STK25 in several different cell types *in vitro*<sup>11,29</sup>; however, the physiological upstream activators of this kinase *in vivo* remain elusive. Interestingly, we found that starvation and challenge with a high-fat diet, which both lead to a shift in fuel metabolism from carbohydrates to fat and increase oxidative stress parameters, markedly and significantly increased the threonine 174 phosphorylation of STK25 in mouse liver (Figure 13B and C).

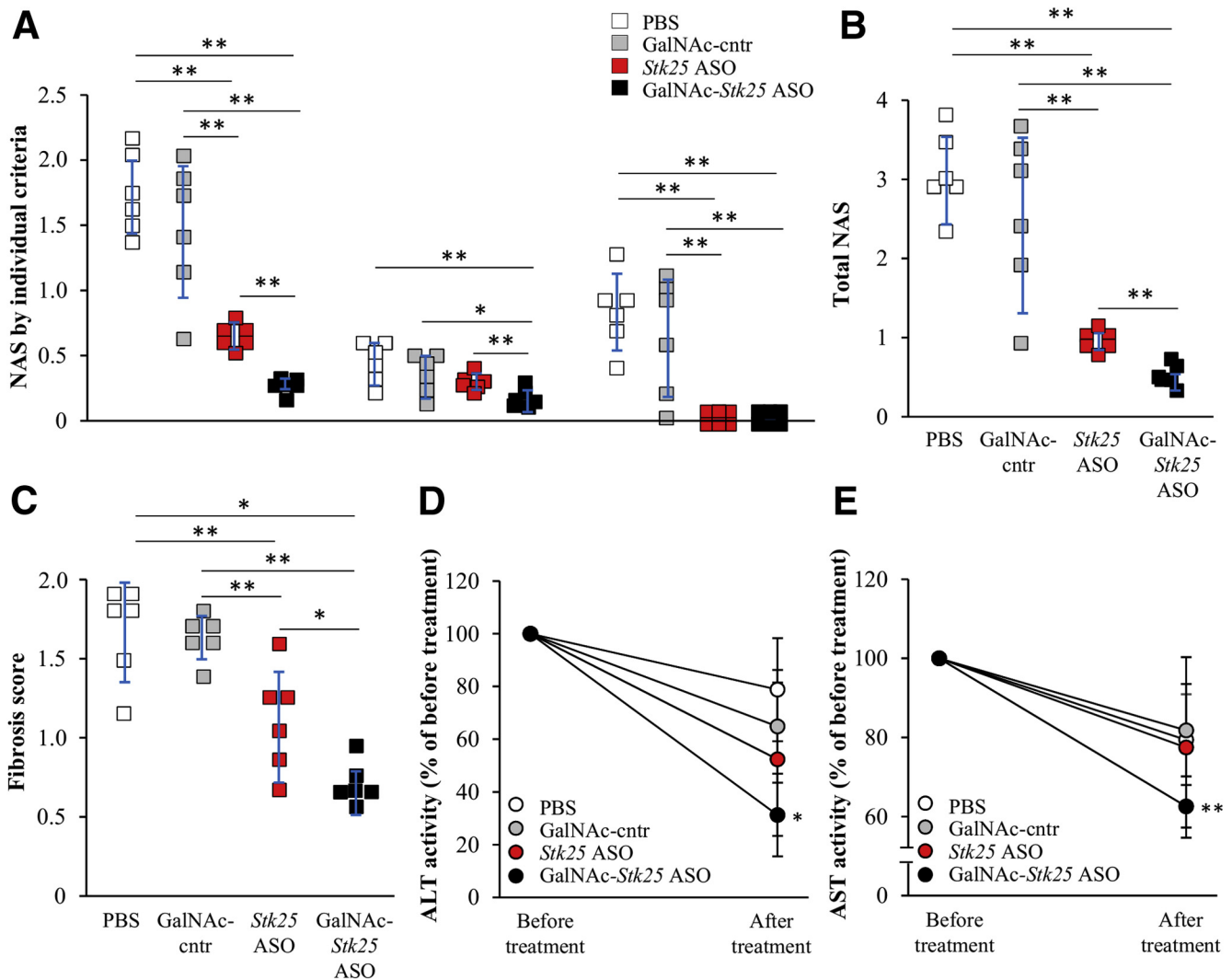
## Discussion

This study found that systemic administration of hepatocyte-targeting GalNAc-conjugated *Stk25* ASO in obese mice effectively ameliorated high-fat-diet-induced steatosis, inflammatory infiltration, hepatic stellate cell activation, nutritional fibrosis, and hepatocellular damage in the liver compared with mice treated with GalNAc-conjugated non-targeting ASO, without any changes in total body weight (Figure 14). The GalNAc-*Stk25* was well tolerated in mice and we observed no systemic toxicity or local tolerability concerns.

Our previous experiments have shown that inhibiting STK25 by treatment with unconjugated parent ASO (ie, the generation 2.5 *Stk25* ASO), which also was used as an internal control in this study, prevents NAFLD

progression in obese mice.<sup>10</sup> Generation 2.5 ASOs, which distribute broadly to peripheral organs including liver, muscle, and adipose tissue,<sup>17</sup> have been widely used in preclinical experimental models<sup>30–33</sup> and currently are being evaluated in various clinical trials.<sup>32,34</sup> In contrast, conjugation of an ASO with a GalNAc moiety, as was applied in this study, targets the ASO selectively to the liver via the GalNAc-binding asialoglycoprotein (ASGP) receptor, a highly conserved C-type lectin that is expressed abundantly on hepatocytes.<sup>18</sup> GalNAc-conjugated ASOs recently have advanced into preclinical and clinical development and the results of early clinical trials evaluating target reduction and safety have been reported for 4 of these ASOs.<sup>35</sup> In line with previously published observations for different targets,<sup>18,36</sup> we here found that conjugation of a GalNAc cluster improved the efficacy of parent unconjugated ASO in repressing *Stk25* levels in the mouse liver by approximately 10-fold. Furthermore, we found that treatment with GalNAc-*Stk25* ASO achieved superior or similar efficacy in reducing diet-induced liver steatosis, inflammation, and fibrosis in mice compared with using 4-fold higher doses of parent unconjugated *Stk25* ASO by an identical administration scheme (6 weeks of treatment fractionated into 2 weekly injections). Thus, this study provides *in vivo* evidence that repression of STK25 levels selectively in hepatocytes is sufficient for the metabolic benefit in ameliorating diet-induced NAFLD.

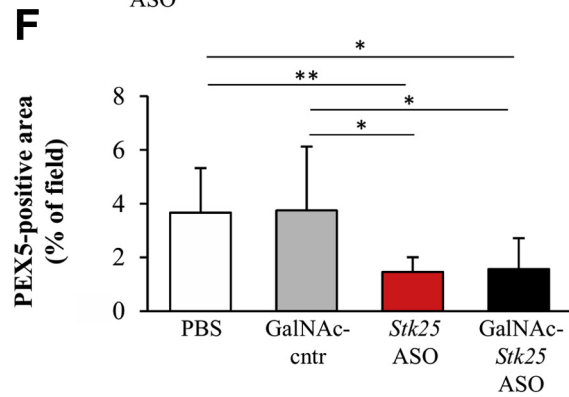
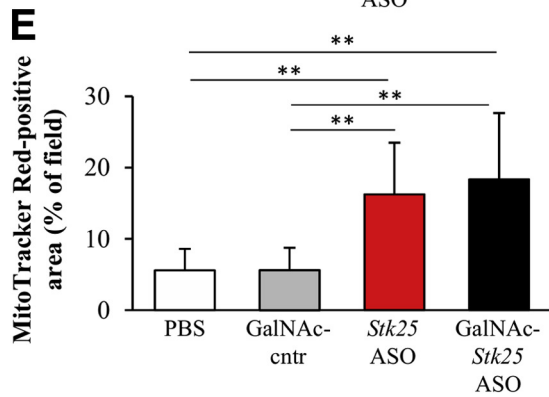
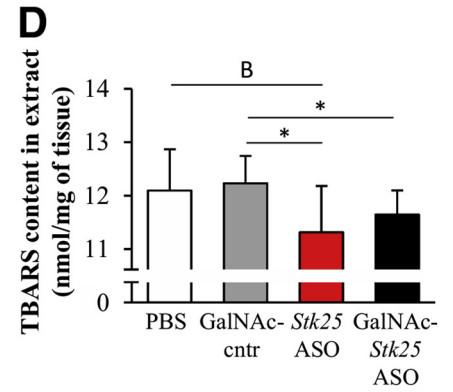
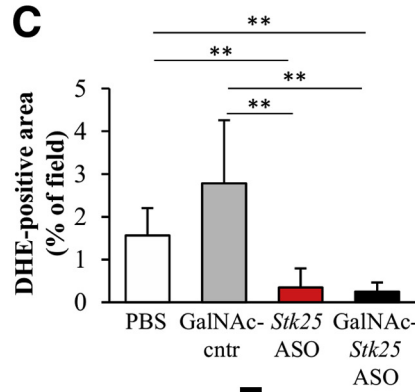
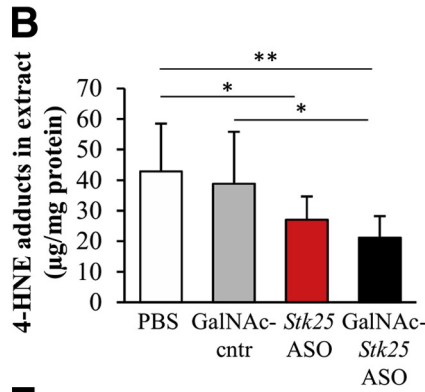
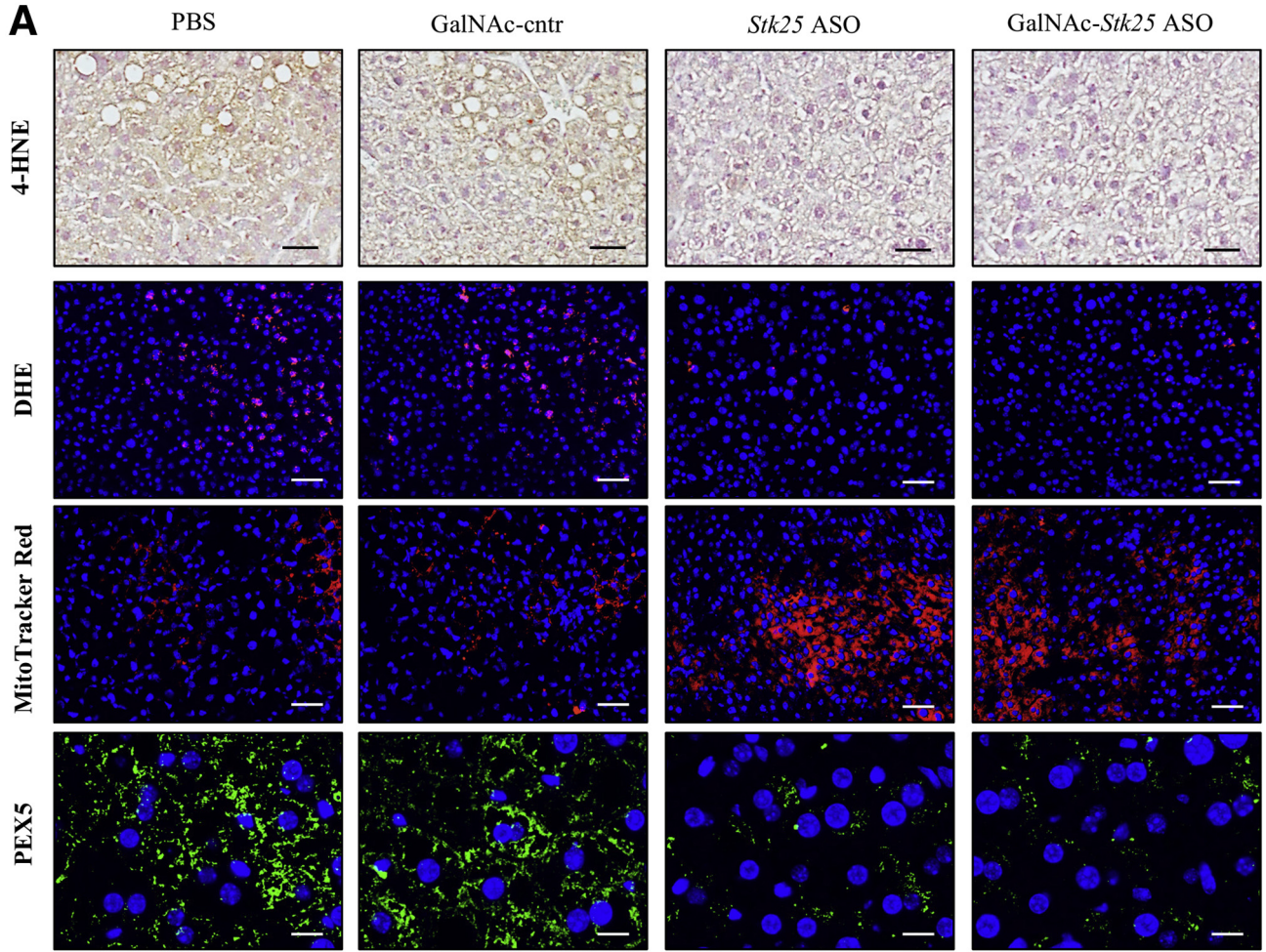
**Figure 9.** (See previous page). Measurement of mRNA expression of selected genes related to (A) hepatic inflammation and (B) fibrosis, as well as genes controlling (C) lipid synthesis and (D) oxidation in the livers from high-fat-fed mice. Mice were treated with GalNAc-*Stk25* ASO (12.5 mg/kg/wk), *Stk25* ASO (50 mg/kg/wk), GalNAc-control ASO (12.5 mg/kg/wk), or placebo (PBS) for 6 weeks. Relative mRNA expression was assessed by quantitative real-time polymerase chain reaction. Data are means  $\pm$  SD ( $n = 6–8$  mice per group) compared with a control group of mice dosed with PBS. Cntr, control. \* $P < .05$ , \*\* $P < .01$ .



**Figure 11. Treatment with GalNAc-*Stk25* ASO reversed high-fat-diet-induced NAFLD in mice.** Mice were treated with GalNAc-*Stk25* ASO (12.5 mg/kg/wk), *Stk25* ASO (50 mg/kg/wk), GalNAc-control ASO (12.5 mg/kg/wk), or placebo (PBS) for 6 weeks. (A and B) Quantification of NAS based on 3 histologic features (steatosis, 0–3; inflammation, 0–3; hepatocellular ballooning, 0–2) in H&E-stained liver sections. (C) Quantification of fibrosis score based on the Kleiner/Brunt criteria adapted to rodents (0, no fibrosis; 1, focal pericellular fibrosis in zone 3; 2, perivenular and pericellular fibrosis confined to zones 2 and 3; 3, bridging fibrosis; and 4, cirrhosis) in liver sections stained with Picrosirius Red. (D and E) Activity of plasma ALT and AST expressed as the ratio of values measured after vs before the treatment in each group. Data are means  $\pm$  SD from (A–C) 6 mice per group or (D and E) 4 mice per group. Cntr, control. \* $P < .05$ , \*\* $P < .01$ .

Interestingly, we found that GalNAc-*Stk25* ASO had a superior effect in obese mice compared with unconjugated parent ASO (*Stk25* ASO) in reducing hepatic steatosis and inflammation measured by NAS scoring of H&E-stained liver sections. In contrast, no difference was detected in hepatic lipids or inflammatory infiltration in mice treated with GalNAc-*Stk25* ASO vs *Stk25* ASO by biochemical measurement of TAG content or assessment of Gr1 (Ly6C)- and F4/80-positive areas in liver, respectively, although a marked and statistically significant improvement was observed in both groups of mice receiving *Stk25*-targeting ASOs compared with the control groups (ie, treatment with PBS or nontargeting control ASO). Furthermore, we observed a significant improvement in histologic fibrosis score assessed in Picrosirius Red-stained liver

sections with GalNAc-*Stk25* ASO vs *Stk25* ASO treatment, although both of these ASOs had similar effects on reducing hepatic fibrosis based on measurements of the collagen I-positive area and hydroxyproline content. Notably, although the same cohort of mice was used in all of these assessments, different regions of the liver were collected for diverse types of analyses: NAS and fibrosis scoring was performed on paraffin sections, immunofluorescence analysis of macrophage markers and collagen I was conducted on frozen sections, whereas TAG and hydroxyproline content was measured in liver homogenate by biochemical assays. Importantly, zonation of glucose and fatty acid metabolism has been reported in the liver lobules according to proximity to the portal triad, such that hepatocytes closest to the portal vein (periportal or zone





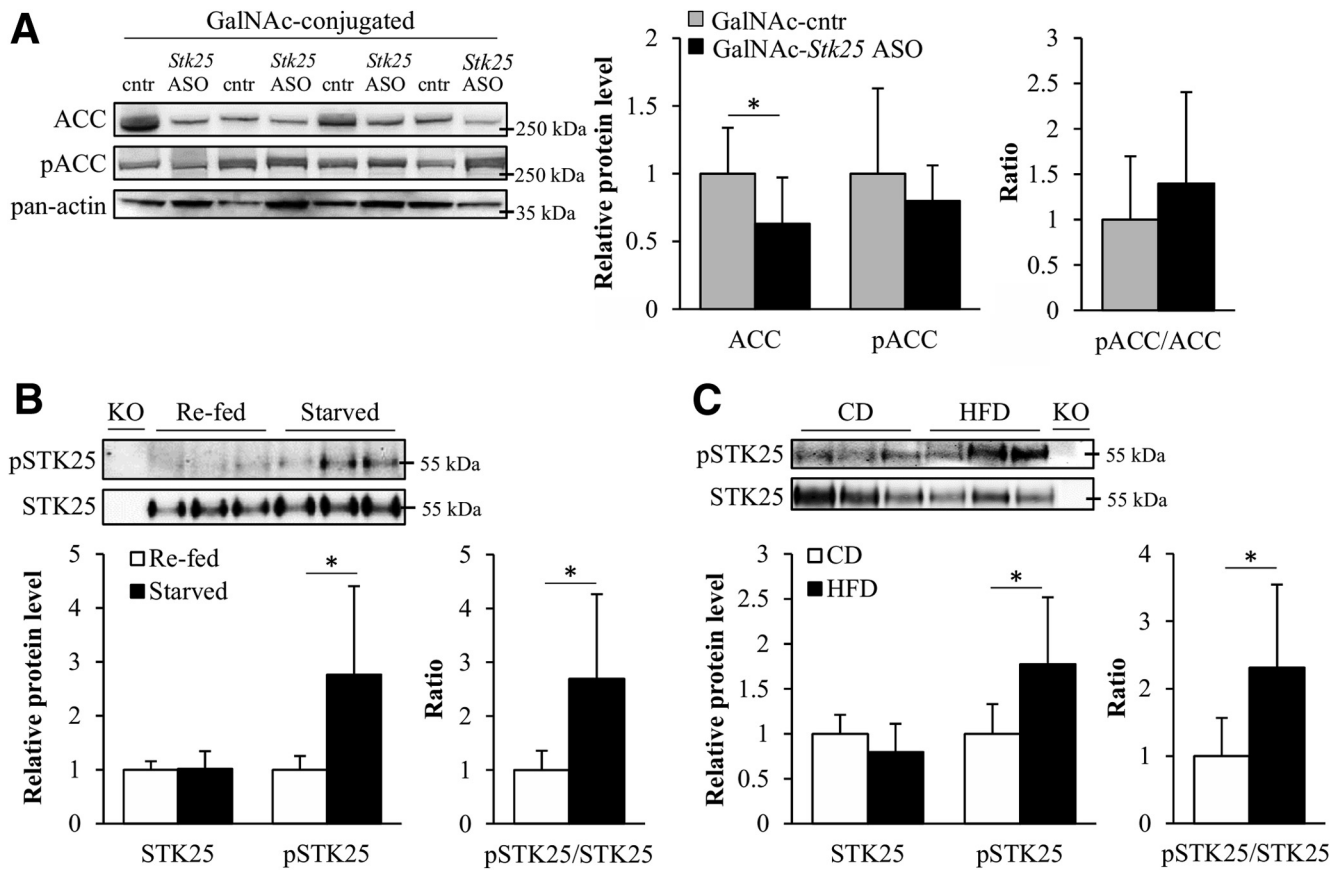


**Figure 13. Downstream targets and upstream activators of STK25.** (A) Liver protein lysates from high-fat-fed mice treated with GalNAc-*Stk25* ASO vs GalNAc-control ASO (12.5 mg/kg/wk) were analyzed by Western blot using antibodies specific for total ACC or phospho-ACC (Ser79), with pan-actin used as a loading control. (B and C) Liver lysates were collected from male C57BL/6J mice (B) fed a normal chow diet and fasted for 12 hours vs re-fed or (C) fed a normal chow diet vs a high-fat diet for 18 weeks. The lysates were immunoprecipitated with anti-STK25 antibody and analyzed by Western blot using antibodies specific for total STK25 or phospho-threonine. Immunoprecipitation of liver lysates from *Stk25* knockout mice was included as a negative control. Protein levels were analyzed by densitometry and data are shown as the total and phospho-protein abundance, as well as the ratio of phospho-protein to total protein. Representative Western blots are shown. Data are means  $\pm$  SD from 6–8 mice per group. Cntr, control. \* $P < .05$ .

1) are more involved in gluconeogenesis and free fatty acid oxidation, whereas glycolysis and lipogenesis occur at a higher rate in hepatocytes closest to the central vein (pericentral or zone 3).<sup>37–39</sup> As a consequence, lipids, inflammation, and hepatocellular damage are distributed differentially within the liver lobules, and steatosis in adult NAFLD and oxidative damage to cells in NASH are localized chiefly to pericentral regions.<sup>37,38</sup> Thus, metabolic zonation of the liver might have contributed to the differences in results observed in this study comparing diverse types of assessments.

Notably, zonal heterogeneity of the ASGP receptor has been reported previously even if the results are not fully consistent. Autoradiography analysis of rat livers perfused ex vivo with the ligand <sup>125</sup>I-asialo-orosomucoid (ASOR) showed a higher uptake by the ASGP receptor in zone 3 than in zone 1 hepatocytes.<sup>40</sup> In contrast, McFarlane et al<sup>41</sup> found that the binding of antibodies to the ASGP receptor was higher in periportal areas in the rat liver. When periportal and perivenous parenchymal cells were isolated from rat livers and incubated in vitro with ASOR, the maximum

**Figure 12. (See previous page). *Stk25*-targeting ASOs efficiently suppressed oxidative stress and improved mitochondrial activity in the livers of obese mice.** Mice were treated with GalNAc-*Stk25* ASO (12.5 mg/kg/wk), *Stk25* ASO (50 mg/kg/wk), GalNAc-control ASO (12.5 mg/kg/wk), or placebo (PBS) for 6 weeks. (A) Representative liver sections processed for immunohistochemistry/immunofluorescence with anti-4-HNE (brown) or anti-PEX5 antibodies (green), or stained with DHE (red) or MitoTracker Red (red); nuclei were stained with DAPI (blue). Scale bars: 50  $\mu$ m for 4-HNE, DHE, and MitoTracker Red, and 12.5  $\mu$ m for PEX5. (B and D) Quantification of (B) 4-HNE adducts and (D) TBARS in liver extract. (C, E, and F) Quantification of (C) DHE, (E) MitoTracker Red, and (F) PEX5 staining. (B–F) Data are means  $\pm$  SD from 6–8 mice per group. Cntr, control. \* $P < .05$ , \*\* $P < .01$ , <sup>B</sup> $P = .087$ .

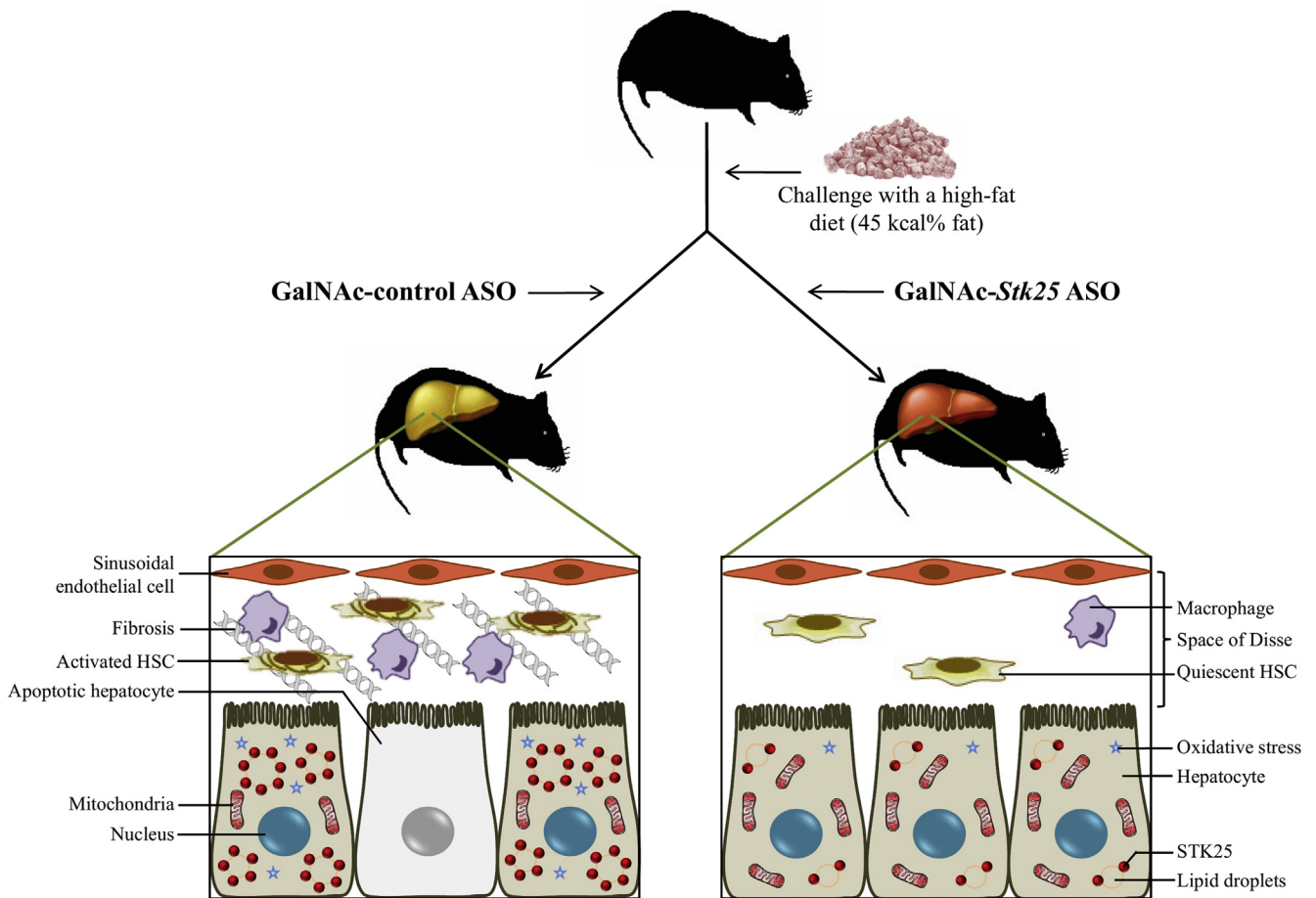


**Figure 14. Schematic illustration of metabolic responses in the liver from mice treated with GalNAc-*Stk25* ASO vs GalNAc-control ASO.** Treatment with hepatocyte-specific GalNAc-conjugated *Stk25* ASO effectively ameliorated high-fat-diet-induced liver steatosis, inflammatory infiltration, hepatic stellate cell (HSC) activation, nutritional fibrosis, and hepatocellular damage compared with mice treated with GalNAc-conjugated nontargeting ASO, without any systemic toxicity or local tolerability concerns.

binding capacity of the ASGP receptor on periportal cells was found to be 0.70 times that of perivenous cells.<sup>42</sup> Furthermore, injection of a small amount of ASOR *in vivo* showed that in young rats binding and uptake occurred predominantly in the periportal area, whereas in older rats a homogeneous distribution over the periportal and perivenous zones was observed.<sup>43</sup> In this study, we have not attempted to systematically analyze the intrahepatic distribution pattern of GalNAc-*Stk25* ASO; however, previous reports showing that ASGP-receptor-dependent uptake pathways are under zonal control suggest the possibility of zonal differences in the repression of STK25 levels by GalNAc-*Stk25* ASO.

Mechanistically, we found decreased mRNA and protein abundance of ACC in the livers from obese mice dosed with GalNAc-*Stk25* ASO vs GalNAc-control ASO. This alteration is expected to reprogram hepatic metabolism, leading to reduced lipid synthesis and increased mitochondrial  $\beta$ -oxidation.<sup>44</sup> These data also confirm our previous findings of lower hepatic ACC levels in *Stk25* knockout mice as well as in mice treated with generation 2.5 *Stk25* ASOs.<sup>6,10</sup>

Notably, several lines of evidence suggest that decreases in mitochondrial functionality, with subsequent increases in oxidative stress, are the leading upstream triggers in transitioning from benign liver steatosis to NASH.<sup>25,26</sup> Here, we observed that treatment with *Stk25*-targeting ASOs protected against liver oxidative damage, as evidenced by reduced levels of hepatic 4-HNE, DHE, and TBARS (classic markers of oxidative stress), and improved mitochondrial function, as evidenced by enhanced MitoTracker Red staining, compared with the control groups of mice. Consistent with these findings, we previously have reported protection against methionine- and choline-deficient diet-induced oxidative stress, as well as functional and ultrastructural impairment in mitochondria, in the livers from *Stk25*<sup>-/-</sup> mice compared with wild-type littermates.<sup>8</sup>

In this study, NAFLD was induced in mice by high-fat diet (45 kcal% fat) feeding for 21 weeks. Most of our previous work characterizing the whole-body function of STK25, as well as its function in other organs such as skeletal muscle, adipose tissue, and pancreas, has been performed using this dietary regimen in genetically

modified mice.<sup>6,7,12-15</sup> Thus, the selected model provides the best basis for comparisons of the metabolic effects of *Stk25* in different organ systems. Still, using a single mouse model is considered to be a limitation of the work and dosing with GalNAc-*Stk25* ASO in a different animal model of NAFLD/NASH would be of high interest to provide further evidence for its efficacy. Furthermore, the detailed toxicology screens (beyond the reported liver/kidney function tests and measurement of organ/body weights in chow-fed lean mice and monitoring the behavior/clinical signs and local injection-site reactions in high-fat-fed mice) have not yet been performed with GalNAc-*Stk25* ASO.

In summary, GalNAc conjugation of *Stk25* ASO provided liver-specific delivery and markedly increased ASO potency in reducing the hepatic target mRNA expression in mice without any safety concerns. Treatment with GalNAc-*Stk25* ASO ameliorated the development and progression of high-fat-diet-induced NAFLD in a mouse model with the effect being similar to, or improved, compared with 4-fold higher doses of unconjugated *Stk25* ASO, which results in broad systemic target reduction. With multiple GalNAc-conjugated ASOs advancing to late stage (phase 2b and phase 3) clinical trials in different therapeutic areas, understanding of the performance of this specialized class of ASOs is expected to broaden in the next few years. With prevention and treatment of NAFLD/NASH remaining a significant unmet medical need, future investigations to address the therapeutic potential of GalNAc-*Stk25* ASO are warranted.

## Materials and Methods

All authors had access to the study data and reviewed and approved the final manuscript.

### Generation of ASOs

The oligonucleotides used in this study were 16 nucleotides in length and chemically modified with phosphorothioates in the backbone, 3 of the 2'-4' constrained ethyl residues at each terminus, and a central deoxynucleotide region of 10 residues (3-10-3 gapmer design). Oligonucleotides were synthesized as previously described.<sup>45</sup> For hepatocyte-targeting ASO, conjugation to GalNAc was performed as previously described.<sup>46</sup> ASO sequences used in this study were as follows: *Stk25* ASO 5'-GCA-TAATCCCCTAGGC-3' and control ASO 5'-GGCCAA-TACGCCGTCA-3'. ASOs were dissolved in PBS (without Ca<sup>2+</sup> or Mg<sup>2+</sup>; Invitrogen, Carlsbad, CA) for in vivo experiments.

### Animal Experiments

Male C57BL/6J mice (Charles River, Sulzfeld, Germany; Jackson, Sacramento, CA) were housed 4–8 per cage in a temperature-controlled (21°C) facility with a 12-hour light-dark cycle with free access to water and food. To compare the efficacy of GalNAc-*Stk25* ASO with parent unconjugated *Stk25* ASO in reducing the target gene expression, 6-week-old mice fed a regular chow diet were administered GalNAc-*Stk25* ASO, *Stk25* ASO, GalNAc-control ASO, or PBS twice weekly for 4 weeks at the indicated total weekly concentrations by subcutaneous injections. At the age of 10 weeks,

the mice were killed. Liver and skeletal muscle samples were snap-frozen in liquid nitrogen and stored at -80°C for analysis of *Stk25* mRNA expression.

To assess the metabolic effect of GalNAc-*Stk25* ASO in comparison with *Stk25* ASO, 6-week-old mice were fed a high-fat diet (45 kcal% fat; D12451; Research Diets, New Brunswick, NJ) for 21 weeks and were treated with GalNAc-*Stk25* ASO (12.5 mg/kg/wk), *Stk25* ASO (50 mg/kg/wk), GalNAc-control ASO (12.5 mg/kg/wk), or placebo (PBS) by intraperitoneal injections twice weekly for the last 6 weeks (Figure 3). Body weight was recorded weekly during the treatment period. At the age of 27 weeks, the mice were killed after 4 hours of food withdrawal. Blood was collected by heart puncture for analysis of ALT and AST activity and glucose and insulin levels. Liver samples were collected for histologic analysis (see later). Liver, gastrocnemius skeletal muscle, and subcutaneous WAT samples also were snap-frozen in liquid nitrogen and stored at -80°C for biochemical assays and/or analysis of gene and protein expression.

Based on the SD of the percentage change in *Stk25* mRNA expression observed in chow-fed lean mice by *Stk25* ASO treatment in our previous study,<sup>10</sup> we estimated that 4 mice per group were required to have 80% power to detect a 60% reduction in target gene expression using a 2-sided test with a 0.05 significance level. Therefore, n = 4 mice per group were included in studies of *Stk25* mRNA levels in lean mice. Our previous experience dictated that larger numbers generally are required to show pharmacologic effects in disease models owing to higher animal-to-animal variability. Therefore, in most of the efficacy assessments performed in high-fat-diet-fed mice, 6–8 mice per treatment group were included.

All animal experiments were performed after prior approval from the local Ethics Committee for Animal Studies at the Administrative Court of Appeals in Gothenburg, Sweden, or by the Institutional Animal Care and Use Committee, Carlsbad, CA, following appropriate guidelines.

### Biochemical Assays

In chow-fed mice, plasma albumin, bilirubin, blood urea nitrogen, creatinine, ALT, and AST levels were measured using the AU480 Clinical Chemistry Analyzer (Beckman Coulter, Providence, RI). In high-fat-fed mice, plasma ALT and AST activity was measured using the ALT Activity Assay Kit (700260; Cayman Chemical, Ann Arbor, MI) and the AST Activity Assay Kit (MAK055; Sigma-Aldrich, St. Louis, MO), respectively. Fasting blood glucose and plasma insulin were assessed using the Accu-Chek glucometer (Roche Diagnostics, Basel, Switzerland) and the Ultrasensitive Mouse Insulin Enzyme-Linked Immunosorbent Assay Kit (90080; Crystal Chem, Downers Grove, IL), respectively. TAG and collagen content were assessed in liver homogenate using the Triglyceride Quantification Colorimetric Kit (K622-100; BioVision, Mountain View, CA) and the Hydroxyproline Colorimetric Assay Kit (MAK008; Sigma-Aldrich), respectively. To characterize hepatic oxidative stress, 4-HNE and TBARS levels in liver homogenate were measured with the OxiSelect HNE Adduct Competitive Enzyme-Linked

Immunosorbent Assay Kit (STA-838; Cell Biolabs, Inc, San Diego, CA) and the Lipid Peroxidation Assay Kit (MAK085; Sigma-Aldrich), respectively.

### Histology

Liver samples were fixed with 4% (vol/vol) phosphate-buffered formaldehyde (Histolab Products, Gothenburg, Sweden), embedded in paraffin, sectioned, and stained with H&E. Ten randomly selected microscopic fields ( $\times 200$ ) per mouse were assessed for NAS according to the Kleiner/Brunt criteria.<sup>20-23</sup> To estimate the degree of fibrosis, liver sections were stained with Picrosirius Red (Histolab Products) and counterstained with Fast Green (Sigma-Aldrich); 10 randomly selected microscopic fields ( $\times 200$ ) per mouse were assessed for fibrosis score according to the Kleiner/Brunt criteria.<sup>20,21,24</sup> Apoptotic cells were detected by terminal deoxynucleotidyl transferase-mediated deoxyuridine triphosphate nick-end labeling assay with the Apo-BrdU-IHC In Situ DNA Fragmentation Assay Kit (K403-50; BioVision).

In parallel, liver samples were embedded in optimal cutting temperature mounting medium (Histolab Products) and frozen in liquid nitrogen, followed by cryosectioning and staining with Oil Red O (Sigma-Aldrich) for neutral lipids. The total hepatic lipid area was quantified in Oil Red O-stained sections in 5 randomly selected microscopic fields ( $\times 200$ ) per mouse using ImageJ software (ImageJ version 1.47; Wayne Rasband National Institutes of Health, Bethesda, MD). Cryosections also were stained with DHE (Life Technologies, Grand Island, NY) to assess oxidative stress or MitoTracker Red (Thermo Fisher Scientific, Waltham, MA) for the detection of respiring mitochondria as previously described.<sup>8</sup> The stained area was quantified in 5 randomly selected microscopic fields ( $\times 200$ ) per mouse using ImageJ software.

The NAS and fibrosis scoring was performed in a blinded fashion by an independent observer; the other analyses were not blinded to treatment allocation.

### Immunohistochemistry and Immunofluorescence

Liver sections were incubated with primary antibodies, followed by incubation with biotinylated secondary antibodies. The following primary antibodies were used: anti-STK25 (YSK1; sc-6865; Santa Cruz Biotechnology, Santa Cruz, CA), anti-PCNA (MA5-1158; Invitrogen), anti-Ki67 (14-5698-82; Invitrogen), anti-Gr1 (Ly6C) (ab15627; Abcam, Cambridge, UK), anti-F4/80 (MCA497GA; Bio-Rad, Hercules, CA), anti-collagen I (SAB4500362; Sigma-Aldrich), anti- $\alpha$ -smooth muscle actin (ab5694; Abcam), anti-4-HNE (sc-130083; Santa Cruz Biotechnology), anti-PEX5 (PA5-58716; Invitrogen), and anti-ubiquitin (ab411; Abcam). For immunohistochemical detection, anti-goat IgG (E0466; Dako, Glostrup, Denmark) and anti-mouse IgG (E0464; Dako) secondary antibodies were used, followed by horseradish-peroxidase-conjugated streptavidin (P0397; Dako) and diaminobenzidine staining (K3467; Dako). For immunofluorescence detection, Alexa Fluor-594-labeled goat anti-rat IgG (A11007; Invitrogen), Alexa Fluor-488-labeled rabbit anti-mouse IgG (A11059; Invitrogen), Alexa Fluor-

594-labeled donkey anti-goat IgG (A11058; Invitrogen), and Alexa Fluor-594-labeled donkey anti-rabbit IgG (A21207; Invitrogen) secondary antibodies were used. The stained area was quantified in 5 randomly selected microscopic fields ( $\times 200$ ) per mouse using ImageJ software.

### Immunoprecipitation

For immunoprecipitation, 100  $\mu$ g of protein from mouse liver lysate was incubated overnight at 4°C with 2  $\mu$ g of anti-STK25 antibody (25821-1-AP; Proteintech, Chicago, IL) coupled with G-coupled Dynabeads (Invitrogen). Immunoprecipitated protein samples were subjected to Western blot (see later).

### Quantitative Real-Time Polymerase Chain Reaction and Western Blot Analysis in Mouse Tissue Samples

RNA was isolated from the liver and skeletal muscle samples with either the EZNA Total RNA Kit (R6834; Omega Bio-Tek, Norcross, GA) or the RNeasy 96 Kit (74182; Qiagen, Hilden, Germany) according to the manufacturer's recommendations, and complementary DNA was synthesized for real-time polymerase chain reaction using the High-Capacity Complementary DNA Reverse Transcription Kit (4368814; Thermo Fisher Scientific). Relative quantification was performed with the QuantStudio 6 Flex System (Applied Biosystems, Foster City, CA) using complementary DNA or the StepOnePlus Real-Time Polymerase Chain Reaction System (Applied Biosystems) using total RNA (see Table 1 for custom-designed primer and probe sequences). Relative quantities of target transcripts were calculated after normalization of the data to the endogenous control, 18S ribosomal RNA (Applied Biosystems), or to total RNA measured by the Quant-iT RiboGreen RNA reagent (Molecular Probes, Eugene, OR).

Western blot on tissue samples was performed as previously described.<sup>47</sup> The detection of specific proteins used the following primary antibodies: anti-STK25, anti-PCNA, anti-Ki67, anti-ACC (#3662; Cell Signaling Technology, Boston, MA), anti-phospho-ACC (Ser79; #3661; Cell Signaling Technology), anti-phospho-threonine (13-9200; Invitrogen), anti-pan-actin (sc-8432; Santa Cruz Biotechnology), anti-glyceraldehyde-3-phosphate-dehydrogenase (MA5-15738; Invitrogen), anti- $\beta$ -actin (ab8226; Abcam), and horseradish-peroxidase-conjugated secondary antibodies anti-rabbit IgG (#7074; Cell Signaling Technology), anti-mouse IgG (#7076; Cell Signaling Technology), anti-rat IgG (#7077; Cell signaling Technology), and VeriBlot for IP Detection Reagent (ab131366; Abcam).

### Measurement of $\beta$ -Oxidation in Mouse Primary Hepatocytes

Primary hepatocytes were isolated using a collagenase perfusion method,<sup>48</sup> pooled from 4 C57BL/6J mice, and seeded on 6-well plates (Nunc, Roskilde, Denmark) at a density of  $5 \times 10^5$  cells/well. The cells were cultured in Williams E medium (Invitrogen) supplemented with 0.28

**Table 1.** Sequences of Custom-Designed Primers and Probes Used for Quantitative Real-Time Polymerase Chain Reaction

Gene	Sequence (5'-3')
<i>Stk25</i>	
Forward	ATCAAGCAGTCGGCCTATGACT
Reverse	CCTTGGCCAGCTCAATGG
Probe	CAAGGCTGACATCTGGTCCCTGGG
<i>F4/80</i>	
Forward	CAAGGACACGAGGTTGCTGA
Reverse	CAAGGGGCCAATCTGGAA
Probe	TGCTCCTGGGTGCTGGGCATT
<i>Ccl2</i>	
Forward	TGGCTCAGCCAGATGCAGT
Reverse	GGACACCTGCTGCTGGTGAT
Probe	TGAGTAGCAGCAGGTGAGTGGGGC
<i>Stat3</i>	
Forward	CCTCCAGACGGCAGCCA
Reverse	TCATTTTCTGTTCTAGATCCTGCAC
Probe	AGCAAGGGGGCCAGGCCAA
<i>Mmp2</i>	
Forward	TGCAGGAGACAAGTTCTGGAGAT
Reverse	ACCCTTGAAGAAGTAGCTATGACCA
Probe	CCGCCCTGCAGGTCCACGAC
<i>Fasn</i>	
Forward	CTTAGCAGAGATCCCGAGACG
Reverse	GGTCCTTTGAAGTGAAGAAGAA
Probe	TGGGCTACAGCATGGTGGGCTG
<i>Cpt1</i>	
Forward	GGGCCATCTGTGGGAGTATG
Reverse	CCTTTACAGTGTCCATTCCTGAGT
Probe	TGGCCGACGTCTTCCAGC
<i>Cy5c</i>	
Forward	GGACCAAACTCTCCACGGTCT
Reverse	CCCCAGGTGATGCCTTTGT
Probe	AGCCTGGCCTGTCTCCGCC
<i>Ucp3</i>	
Forward	ACTGACAACCTCCCTGTCACTT
Reverse	GCGTTCATGTATCGGGTCTTTA
Probe	ACAGTGGTGGCCTCCCCGGTG

mol/L sodium ascorbate (Sigma-Aldrich), 0.1 mmol/L sodium selenite (Sigma-Aldrich), 100 mg/mL penicillin and 100 U/mL streptomycin (Gibco Invitrogen Corporation, Paisley, Scotland), 3 g/L glucose (Sigma-Aldrich), and 26 IU/L insulin (Novo Nordisk, Bagsværd, Denmark). Cells were treated with 1000 nmol/L GalNAc-control ASO or GalNAc-*Stk25* ASO for 24 hours. To measure  $\beta$ -oxidation, cells were incubated in the presence of (9,10-<sup>3</sup>H[N])-palmitic acid, and (<sup>3</sup>H)-labeled water was measured as the product of free fatty acid oxidation.<sup>9</sup>

### Statistical Analysis

Statistical significance between the groups was evaluated using the 2-sample Student *t* test, and among more than 2 groups by 1-way analysis of variance followed by a 2-sample Student *t* test for post hoc analysis. The Shapiro-Wilk test and the Levene test were applied to confirm the normality of distribution of residuals and the homogeneity of variances, respectively. Differences were considered statistically significant at a *P* value less than

.05. All statistical analyses were performed using SPSS Statistics (v24; IBM Corporation, Armonk, NY).

### References

1. Younossi Z, Anstee QM, Marietti M, Hardy T, Henry L, Eslam M, George J, Bugianesi E. Global burden of NAFLD and NASH: trends, predictions, risk factors and prevention. *Nat Rev Gastroenterol Hepatol* 2018; 15:11–20.
2. Younossi ZM, Koenig AB, Abdelatif D, Fazel Y, Henry L, Wymer M. Global epidemiology of nonalcoholic fatty liver disease-meta-analytic assessment of prevalence, incidence, and outcomes. *Hepatology* 2016;64:73–84.
3. Anstee QM, Targher G, Day CP. Progression of NAFLD to diabetes mellitus, cardiovascular disease or cirrhosis. *Nat Rev Gastroenterol Hepatol* 2013;10:330–344.
4. Trebicka J, Schierwagen R. Hepatic mitochondrial dysfunction in nonalcoholic steatohepatitis: read-out or reason? *Hepatology* 2016;63:1729–1732.
5. Thompson BJ, Sahai E. MST kinases in development and disease. *J Cell Biol* 2015;210:871–882.
6. Amrutkar M, Cansby E, Chursa U, Nunez-Duran E, Chanclon B, Stahlman M, Friden V, Manneras-Holm L, Wickman A, Smith U, Backhed F, Boren J, Howell BW, Mahlapuu M. Genetic disruption of protein kinase STK25 ameliorates metabolic defects in a diet-induced type 2 diabetes model. *Diabetes* 2015;64:2791–2804.
7. Amrutkar M, Cansby E, Nunez-Duran E, Pirazzi C, Stahlman M, Stenfeldt E, Smith U, Boren J, Mahlapuu M. Protein kinase STK25 regulates hepatic lipid partitioning and progression of liver steatosis and NASH. *FASEB J* 2015;29:1564–1576.
8. Amrutkar M, Chursa U, Kern M, Nunez-Duran E, Stahlman M, Sutt S, Boren J, Johansson BR, Marschall HU, Bluher M, Mahlapuu M. STK25 is a critical determinant in nonalcoholic steatohepatitis. *FASEB J* 2016;30:3628–3643.
9. Amrutkar M, Kern M, Nunez-Duran E, Stahlman M, Cansby E, Chursa U, Stenfeldt E, Boren J, Bluher M, Mahlapuu M. Protein kinase STK25 controls lipid partitioning in hepatocytes and correlates with liver fat content in humans. *Diabetologia* 2016;59:341–353.
10. Nunez-Duran E, Aghajan M, Amrutkar M, Sutt S, Cansby E, Booten SL, Watt A, Stahlman M, Stefan N, Haring HU, Staiger H, Boren J, Marschall HU, Mahlapuu M. Serine/threonine protein kinase 25 anti-sense oligonucleotide treatment reverses glucose intolerance, insulin resistance, and nonalcoholic fatty liver disease in mice. *Hepatol Commun* 2018;2:69–83.
11. Nerstedt A, Cansby E, Andersson CX, Laakso M, Stancakova A, Bluher M, Smith U, Mahlapuu M. Serine/threonine protein kinase 25 (STK25): a novel negative regulator of lipid and glucose metabolism in rodent and human skeletal muscle. *Diabetologia* 2012; 55:1797–1807.
12. Cansby E, Amrutkar M, Manneras Holm L, Nerstedt A, Reyahi A, Stenfeldt E, Boren J, Carlsson P, Smith U, Zierath JR, Mahlapuu M. Increased expression of STK25 leads to impaired glucose utilization and insulin

- sensitivity in mice challenged with a high-fat diet. *FASEB J* 2013;27:3660–3671.
13. Chursa U, Nunez-Duran E, Cansby E, Amrutkar M, Sutt S, Stahlman M, Olsson BM, Boren J, Johansson ME, Backhed F, Johansson BR, Sihlbom C, Mahlapuu M. Overexpression of protein kinase STK25 in mice exacerbates ectopic lipid accumulation, mitochondrial dysfunction and insulin resistance in skeletal muscle. *Diabetologia* 2017;60:553–567.
  14. Nunez-Duran E, Chanclon B, Sutt S, Real J, Marschall HU, Wernstedt Asterholm I, Cansby E, Mahlapuu M. Protein kinase STK25 aggravates the severity of non-alcoholic fatty pancreas disease in mice. *J Endocrinol* 2017;234:15–27.
  15. Sütt S, Cansby E, Paul A, Amrutkar M, Nunez-Duran E, Kulkarni NM, Ståhlman M, Borén J, Laurencikiene J, Howell BW, Enerbäck S, Mahlapuu M. STK25 regulates oxidative capacity and metabolic efficiency in adipose tissue. *J Endocrinol* 2018;238:187–202.
  16. Cansby E, Magnusson E, Nunez-Duran E, Amrutkar M, Pedrelli M, Parini P, Hoffmann J, Stahlman M, Howell BW, Marschall HU, Boren J, Mahlapuu M. STK25 Regulates cardiovascular disease progression in a mouse model of hypercholesterolemia. *Arterioscler Thromb Vasc Biol* 2018;38:1723–1737.
  17. Hung G, Xiao X, Peralta R, Bhattacharjee G, Murray S, Norris D, Guo S, Monia BP. Characterization of target mRNA reduction through in situ RNA hybridization in multiple organ systems following systemic antisense treatment in animals. *Nucleic Acid Ther* 2013; 23:369–378.
  18. Prakash TP, Graham MJ, Yu J, Carty R, Low A, Chappell A, Schmidt K, Zhao C, Aghajani M, Murray HF, Riney S, Booten SL, Murray SF, Gaus H, Crosby J, Lima WF, Guo S, Monia BP, Swayze EE, Seth PP. Targeted delivery of antisense oligonucleotides to hepatocytes using triantennary N-acetyl galactosamine improves potency 10-fold in mice. *Nucleic Acids Res* 2014;42:8796–8807.
  19. Tacke F, Zimmermann HW. Macrophage heterogeneity in liver injury and fibrosis. *J Hepatol* 2014;60:1090–1096.
  20. Takahashi Y, Soejima Y, Fukusato T. Animal models of nonalcoholic fatty liver disease/nonalcoholic steatohepatitis. *World J Gastroenterol* 2012;18:2300–2308.
  21. Kleiner DE, Brunt EM, Van Natta M, Behling C, Contos MJ, Cummings OW, Ferrell LD, Liu YC, Torbenson MS, Unalp-Arida A, Yeh M, McCullough AJ, Sanyal AJ; Nonalcoholic Steatohepatitis Clinical Research Network. Design and validation of a histological scoring system for nonalcoholic fatty liver disease. *Hepatology* 2005;41:1313–1321.
  22. Xie L, Yui J, Hatori A, Yamasaki T, Kumata K, Wakizaka H, Yoshida Y, Fujinaga M, Kawamura K, Zhang MR. Translocator protein (18 kDa), a potential molecular imaging biomarker for non-invasively distinguishing non-alcoholic fatty liver disease. *J Hepatol* 2012;57:1076–1082.
  23. Chen L, Shu Y, Liang X, Chen EC, Yee SW, Zur AA, Li S, Xu L, Keshari KR, Lin MJ, Chien HC, Zhang Y, Morrissey KM, Liu J, Ostrem J, Younger NS, Kurhanewicz J, Shokat KM, Ashrafi K, Giacomini KM. OCT1 is a high-capacity thiamine transporter that regulates hepatic steatosis and is a target of metformin. *Proc Natl Acad Sci U S A* 2014;111:9983–9988.
  24. Behari J, Yeh TH, Krauland L, Otruba W, Ciepły B, Hauth B, Apte U, Wu T, Evans R, Monga SP. Liver-specific beta-catenin knockout mice exhibit defective bile acid and cholesterol homeostasis and increased susceptibility to diet-induced steatohepatitis. *Am J Pathol* 2010;176:744–753.
  25. Schuster S, Cabrera D, Arrese M, Feldstein AE. Triggering and resolution of inflammation in NASH. *Nat Rev Gastroenterol Hepatol* 2018;15:349–364.
  26. Koliaki C, Szendroedi J, Kaul K, Jelenik T, Nowotny P, Jankowiak F, Herder C, Carstensen M, Krausch M, Knoefel WT, Schlensak M, Roden M. Adaptation of hepatic mitochondrial function in humans with non-alcoholic fatty liver is lost in steatohepatitis. *Cell Metab* 2015;21:739–746.
  27. Browning JD, Horton JD. Molecular mediators of hepatic steatosis and liver injury. *J Clin Invest* 2004;114:147–152.
  28. Savage DB, Choi CS, Samuel VT, Liu ZX, Zhang D, Wang A, Zhang XM, Cline GW, Yu XX, Geisler JG, Bhanot S, Monia BP, Shulman GI. Reversal of diet-induced hepatic steatosis and hepatic insulin resistance by antisense oligonucleotide inhibitors of acetyl-CoA carboxylases 1 and 2. *J Clin Invest* 2006;116:817–824.
  29. Preisinger C, Short B, De Corte V, Bruyneel E, Haas A, Kopajtich R, Gettemans J, Barr FA. YSK1 is activated by the Golgi matrix protein GM130 and plays a role in cell migration through its substrate 14-3-3zeta. *J Cell Biol* 2004;164:1009–1020.
  30. Donner AJ, Yeh ST, Hung G, Graham MJ, Crooke RM, Mullick AE. CD40 Generation 2.5 antisense oligonucleotide treatment attenuates doxorubicin-induced nephropathy and kidney inflammation. *Mol Ther Nucleic Acids* 2015;4:e265.
  31. Yamamoto Y, Lorient Y, Beraldi E, Zhang F, Wyatt AW, Al Nakouzi N, Mo F, Zhou T, Kim Y, Monia BP, MacLeod AR, Fazli L, Wang Y, Collins CC, Zoubeidi A, Gleave M. Generation 2.5 antisense oligonucleotides targeting the androgen receptor and its splice variants suppress enzalutamide-resistant prostate cancer cell growth. *Clin Cancer Res* 2015;21:1675–1687.
  32. Hong D, Kurzrock R, Kim Y, Woessner R, Younes A, Nemunaitis J, Fowler N, Zhou T, Schmidt J, Jo M, Lee SJ, Yamashita M, Hughes SG, Fayad L, Piha-Paul S, Nadella MV, Mohseni M, Lawson D, Reimer C, Blakey DC, Xiao X, Hsu J, Revenko A, Monia BP, MacLeod AR. AZD9150, a next-generation antisense oligonucleotide inhibitor of STAT3 with early evidence of clinical activity in lymphoma and lung cancer. *Sci Transl Med* 2015;7:314ra185.
  33. Ross SJ, Revenko AS, Hanson LL, Ellston R, Staniszewska A, Whalley N, Pandey SK, Revill M, Rooney C, Buckett LK, Klein SK, Hudson K, Monia BP, Zinda M, Blakey DC, Lyne PD, Macleod AR. Targeting KRAS-dependent tumors with AZD4785, a high-affinity therapeutic antisense oligonucleotide inhibitor of KRAS. *Sci Transl Med* 2017;9.

34. MacLeod AR, Crooke ST. RNA therapeutics in oncology: advances, challenges, and future directions. *J Clin Pharmacol* 2017;57(Suppl 10):S43–S59.
35. Crooke ST, Witztum JL, Bennett CF, Baker BF. RNA-targeted therapeutics. *Cell Metab* 2018;27:714–739.
36. Huang Y. Preclinical and clinical advances of GalNAc-decorated nucleic acid therapeutics. *Mol Ther Nucleic Acids* 2017;6:116–132.
37. Hall Z, Bond NJ, Ashmore T, Sanders F, Ament Z, Wang X, Murray AJ, Bellafante E, Virtue S, Vidal-Puig A, Allison M, Davies SE, Koulman A, Vacca M, Griffin JL. Lipid zonation and phospholipid remodeling in nonalcoholic fatty liver disease. *Hepatology* 2017;65:1165–1180.
38. Yeh MM, Brunt EM. Pathological features of fatty liver disease. *Gastroenterology* 2014;147:754–764.
39. Gebhardt R. Metabolic zonation of the liver: regulation and implications for liver function. *Pharmacol Ther* 1992;53:275–354.
40. van der Sluijs P, Braakman I, Meijer DK, Groothuis GM. Heterogeneous acinar localization of the asialoglycoprotein internalization system in rat hepatocytes. *Hepatology* 1988;8:1521–1529.
41. McFarlane BM, Sipos J, Gove CD, McFarlane IG, Williams R. Antibodies against the hepatic asialoglycoprotein receptor perfused in situ preferentially attach to periportal liver cells in the rat. *Hepatology* 1990;11:408–415.
42. Voorschuur AH, Kuiper J, Neelissen JA, Boers W, Van Berkel TJ. Different zonal distribution of the asialoglycoprotein receptor, the alpha 2-macroglobulin receptor/low-density-lipoprotein receptor-related protein and the lipoprotein-remnant receptor of rat liver parenchymal cells. *Biochem J* 1994;303:809–816.
43. Daniels CK, Smith KM, Schmucker DL. Asialoorosomucoid hepatobiliary transport is unaltered by the loss of liver asialoglycoprotein receptors in aged rats. *Proc Soc Exp Biol Med* 1987;186:246–250.
44. Samuel VT, Shulman GI. Nonalcoholic fatty liver disease as a nexus of metabolic and hepatic diseases. *Cell Metab* 2018;27:22–41.
45. Seth PP, Siwkowski A, Allerson CR, Vasquez G, Lee S, Prakash TP, Wancewicz EV, Witchell D, Swayze EE. Short antisense oligonucleotides with novel 2'-4' conformationally restricted nucleoside analogues show improved potency without increased toxicity in animals. *J Med Chem* 2009;52:10–13.
46. Prakash TP, Yu J, Migawa MT, Kinberger GA, Wan WB, Ostergaard ME, Carty RL, Vasquez G, Low A, Chappell A, Schmidt K, Aghajan M, Crosby J, Murray HM, Booten SL, Hsiao J, Soriano A, Machemer T, Cauntay P, Burel SA, Murray SF, Gaus H, Graham MJ, Swayze EE, Seth PP. Comprehensive structure-activity relationship of triantennary N-acetylgalactosamine conjugated antisense oligonucleotides for targeted delivery to hepatocytes. *J Med Chem* 2016;59:2718–2733.
47. Nerstedt A, Johansson A, Andersson CX, Cansby E, Smith U, Mahlapuu M. AMP-activated protein kinase inhibits IL-6-stimulated inflammatory response in human liver cells by suppressing phosphorylation of signal transducer and activator of transcription 3 (STAT3). *Diabetologia* 2010;53:2406–2416.
48. Quistorff B, Dich J, Grunnet N. Preparation of isolated rat liver hepatocytes. *Methods Mol Biol* 1990;5:151–160.

---

Received October 1, 2018. Accepted December 11, 2018.

#### Correspondence

Address correspondence to: Margit Mahlapuu, PhD, Department of Chemistry & Molecular Biology, The Faculty of Science at University of Gothenburg, Medicinaregatan 9C, SE-413 90 Gothenburg, Sweden. e-mail: Margit.Mahlapuu@gu.se; fax: (46) 31 7862599.

#### Acknowledgments

The authors acknowledge the technical assistance of Ingrid Wernstedt-Asterholm, Institute of Neuroscience and Physiology, University of Gothenburg, Gothenburg, Sweden.

#### Author contributions

Emmelie Cansby, Esther Nuñez-Durán, Elin Magnusson, and Sheri L. Booten generated the bulk of the results; Manoj Amrutkar performed nonalcoholic fatty liver disease activity scoring and fibrosis scoring; Nagaraj M. Kulkarni performed quantitative reverse-transcription polymerase chain reaction analysis; Mariam Aghajan, Hanns-Ulrich Marschall, Jan Borén, and L. Thomas Svensson provided expertise and key reagents, and contributed to the discussion; Margit Mahlapuu directed the project, designed the study, interpreted the data, and wrote the manuscript; and all the authors revised the article critically for important intellectual content and approved the final version of the article to be published.

#### Conflicts of interest

The authors disclose no conflicts.

#### Funding

This work was supported by grants from the Swedish Research Council, the European Foundation for the Study of Diabetes/Lilly European Diabetes Research Programme, the West Sweden Avtal om Läkarutbildning och Forskning (ALF) Program, the Novo Nordisk Foundation, the Swedish Heart-Lung Foundation, the Torsten Söderbergs Foundation, the Diabetes Wellness Network Sweden, the Swedish Diabetes Foundation, the Royal Society of Arts and Sciences in Gothenburg, the Wiberg Foundation, the Adlerbert Research Foundation, the I. Hultman Foundation, the S. and E. Goljes Foundation, the F. Neubergh Foundation, the N. Svarts foundation, the L. and J. Grönbergs Foundation, and the I.-B. and A. Lundbergs Research Foundation.